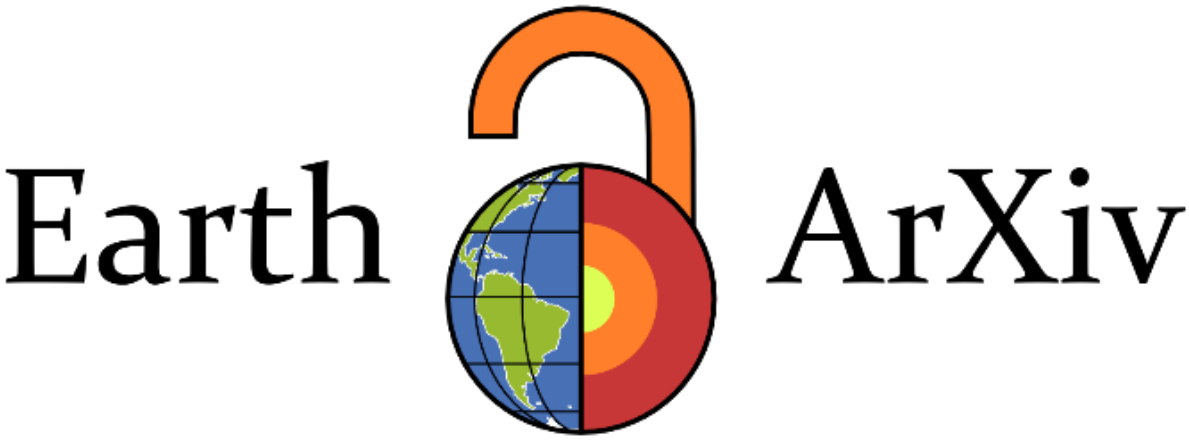

Transformation of climatologically anomalous water masses

Ran Liu,[a] Gaël Forget,[b] Zijie Zhao,[a] Henri F. Drake,[a]

[a] *Department of Earth System Sciences, University of California, Irvine,* [b] *Department of Earth, Atmospheric and Planetary Sciences, Massachusetts Institute of Technology, Cambridge*

Corresponding author: Ran Liu, rliu.ocean@gmail.com

ABSTRACT: We derive a novel anomalous water mass budget framework in which water masses are defined by bounds on tracer anomalies rather than absolute tracer values, extending Water Mass Transformation (WMT) theory to ocean variability and extremes. The material derivative of tracer anomalies introduces three additional transformation terms absent from the standard WMT framework: advection of climatological tracer gradients by velocity anomalies, the convergence of climatological-mean transient advective heat fluxes, and contributions from time mean tendency. The framework is first tested using an analytical model, confirming budget closure and providing a clear physical interpretation of each term. Application to the ECCOv4r4 ocean state estimate over 1993–2017 then reveals that the global volume of anomalously warm water (defined by $\Theta' \geq 3.5^{\circ}$C) exhibits two prominent peaks coinciding with the 1997/98 and 2015/16 El Niño events. Budget analysis identifies anomalous advection of the climatological temperature gradient by velocity anomalies as the dominant driver of warm water volume variability, consistent with the Bjerknes feedback mechanism, while surface heat flux anomalies consistently act as a damping term throughout both events, and other terms are relatively small. Negligibly small residuals confirm the numerical consistency of the framework when applied to a dynamically consistent ocean state estimate. These results establish the budget of anomalous water mass as a rigorous theoretical framework that opens new avenues for systematically investigating the dynamical mechanisms governing the generation, evolution, and dissipation of ocean anomalies associated with climate variability and extreme events.

SIGNIFICANCE STATEMENT: Marine heatwaves and temperature variability in the ocean have significant ecological and climate impacts, yet their physical drivers remain difficult to quantify. Traditional temperature budget approaches often struggle to capture the evolution of extreme anomalies, especially below the surface. Here, we introduce a new framework based on anomalous water mass budgets, which enables a systematic quantification of the processes governing the formation, maintenance, and decay of temperature anomalies. Applying this framework to a global ocean state estimate, we show that extreme warm anomalies are primarily driven by circulation changes acting on the background temperature structure, while moderate anomalies reflect a balance among multiple processes. This approach provides a new pathway for understanding and diagnosing ocean temperature variability and extremes across a wide range of spatial and temporal scales.

1. Introduction

Water masses are bodies of seawater defined by a combination of bounding scalar tracer concentrations or characteristics and using fixed regions of the ocean (Iselin 1939; Sverdrup et al. 1942; Montgomery 1958; Worthington 1959). Using tracers in this fashion, a wide variety of water masses can be identified: density-based definitions yield classic water masses such as North Atlantic Deep Water (NADW) and Antarctic Bottom Water (AABW); temperature-based criteria identify features such as the Western Pacific Warm Pool and the Eastern Pacific cold tongue; potential vorticity-based definitions delineate intermediate and mode waters; and dissolved oxygen-based criteria identify oxygen minimum zones such as those in the Eastern Tropical Pacific. Generally, characterizing the mean state, intrinsic variability, and forced changes of the global ocean, as well as for assessing the long-term impacts of anthropogenic climate change on ocean, can be greatly facilitated by partitioning the ocean into distinct water masses and diagnosing their respective steady-state balances, seasonal cycle, or transient evolutions (Iselin 1939; Sverdrup et al. 1942; Worthington 1959; Speer 1993; Bindoff et al. 2007; Forget et al. 2011; Speer and Forget 2013).

In water mass analysis, ocean variability and change are understood as the variability and change of the constituent water masses. Since oceanographers commonly assume seawater to be incompressible (with a constant reference density), water mass change is equivalent to a change in volume, which occurs when the isoscalar surfaces that define the water mass move through space

(Drake et al. 2025). Early water mass analyses (Iselin 1939; Sverdrup et al. 1942; Worthington 1959; Talley and McCartney 1982) primarily focused on the climatological mean state, identifying and tracking water masses defined by fixed thermohaline criteria on isopycnal surfaces (Talley and McCartney 1982). A major conceptual advance was the introduction of Water Mass Transformation (WMT) theory by Walin (1982), which provides a concise budget equation directly relating the evolution of a water mass' volume to diascalar volume fluxes across isoscalar surfaces, boundary fluxes, and interior mixing processes (Forget et al. 2011; Groeskamp et al. 2019). The WMT approach has further been extended to quantify spurious numerical mixing in ocean models (Nurser et al. 1999; Drake et al. 2025). Even more recently, WMT theory has been applied to the study of extreme climate events, such as diagnosing the volume budget of extreme warm water masses associated with marine heatwaves (Bailey et al. 2024). These analyses have proven invaluable for elucidating the large-scale ocean circulation, ventilation pathways, and the role of the ocean in the global climate system.

Since existing WMT frameworks define water masses based on absolute tracer values (e.g. temperature), they are awkward to apply to problems related to climate variability or extremes, which inherently involve tracer anomalies (e.g. temperature fluctuations relative to a seasonal climatology). With the backdrop of anthropogenic climate change and climate variability, many oceanographic phenomena of scientific and societal interest are identified as anomalies : El Niño-Southern Oscillation (ENSO) is characterized by anomalous sea surface temperatures in the tropical Pacific (Trenberth 1997); marine heatwaves are defined by persistent positive temperature anomalies (Hobday et al. 2016). Although some studies have attempted anomalous transformation budgets of water masses (Speer and Forget 2013; Bailey et al. 2023), this approach is fundamentally based on a static threshold of λ, as opposed to the anomaly λ' of a tracer.

Precisely characterizing the life cycle of water masses defined by anomalies — their formation, growth, and decay — and quantitatively attributing their evolution to specific dynamical processes therefore requires a dedicated theoretical framework. To this end, we derive a novel anomalous water mass budget framework in which water masses are defined by bounds on tracer anomalies rather than absolute tracer values. The framework is first validated against an analytical solution to establish its theoretical consistency and to identify potential sources of numerical error, and then applied to the dynamically consistent ECCOv4r4 ocean state estimate (Forget et al. 2015;

Fukumori et al. 2021) to diagnose the processes governing the variability of global anomalous warm water masses.

The remainder of this paper is organized as follows. Section2 presents the theoretical derivation of the anomalous water mass budget framework under the Boussinesq approximation. Section3 validates the framework against an analytical case, demonstrating its theoretical consistency. Section4 applies the framework to the ECCOv4r4 ocean state estimate to diagnose the processes governing the variability of global anomalous warm water masses. Section5 summarizes the findings and discusses future directions. Appendix A reviews the standard derivation of the water mass transformation budget for an arbitrary tracer. Appendix B describes the configuration and numerical algorithm details of the analytical case. Appendix C presents the derivation of the anomalous water mass transformation budget in the context of the z^* coordinate system employed by ECCOv4r4.

2. Theory

a. Water mass transformation

Before formulating a theory for the transformation of *anomalous* water masses, we briefly review the general Water Mass Transformation (WMT) budget for an arbitrary tracer λ. This general result establishes the kinematic framework used below and is independent of any mean–anomaly decomposition. We define the water mass, $\mathcal{M}_{\geq}$, as the mass of the body of water $\Omega_{\geq}(\lambda, t)$ that has tracer values greater than or equal to a given tracer value λ and is confined to a region of interest $\mathcal{R}$ (Fig. 1a):

$$\mathcal{M}_{\geq}(\lambda, t) = \int_{\Omega_{\geq}(\lambda,t)} \rho \, dV. \tag{1}$$

Walin's (1977) pioneering analysis demonstrated that the mass and tracer conservation equations can be combined to derive a quasi-Lagrangian evolution equation for the water mass $\mathcal{M}_{\geq}$. In Appendix A, we review Drake et al.'s (2025) approach to this derivation, which we use as the basis for extending the framework to tracer anomalies. The ultimate result is the closed budget (Fig. 1a):

$$\frac{\partial}{\partial t}\mathcal{M}_{\geq}(\lambda, t) = \mathcal{S}_{\geq}(\lambda, t) + \Psi_{\geq}(\lambda, t) + \mathcal{G}_M(\lambda, t), \tag{2}$$

where $\mathcal{S}_{\geq}$ is the total surface mass flux into the body of water, $\Psi_{\geq}$ is the total transport of water with tracer values greater than λ across the region's boundary ∂R, and

$$\mathcal{G}_{\geq}(\lambda, t) \equiv -\partial_{\lambda} \int_{\Omega_{\geq} \cap R} \frac{D\lambda}{Dt} \, dV \tag{3}$$

is the water mass transformation rate, which depends on material derivative of the tracer,

$$\frac{D\lambda}{Dt} = \dot{\lambda}. \tag{4}$$

What makes the water mass transformation framework a powerful scientific tool is that the total tracer tendencies $\dot{\lambda}$ on the right-hand-side (RHS) of Eq. (4) can be decomposed to evaluate contributions from the various physical (or biogeochemical) processes that cause water mass transformations.

b. Anomalous Transformation of Water Masses and Transformation of Anomalous Water Masses

Since the seasonal cycle is such a dominant signal of variability for most tracers, it is often useful to instead consider their anomalies λ' relative to a climatological mean $\overline{\lambda}$, where the climatological mean $\overline{(\cdot)}$ is generally computed by phase-averaging over several years and the anomaly is defined as the deviation of the instantaneous field from the climatology, $(\cdot)' = (\cdot) - \overline{(\cdot)}$.

Along these lines, the WMT framework has been adapted to climate variability problems by considering the anomalous WMT budget:

$$\left(\frac{\partial}{\partial t} \mathcal{M}_{\geq}(\lambda) \right)' = (\mathcal{S}_{\geq}(\lambda))' + (\Psi_{\geq}(\lambda))' + (\mathcal{G}_M(\lambda))'. \tag{5}$$

For example, Speer and Forget (2013) consider the seasonal transformation of mode waters and Bailey et al. (2023) consider the climatologically anomalous evolution of waters denser than about $\sigma_2 = 1037.15$ kg/m^3 in the Weddell Sea, which they identify as a precursor of Antarctic Bottom Waters. However, the utility of this approach is limited because the underlying water masses are still defined based on a static threshold of λ, resulting in an awkward mismatch between the theoretical framework (in terms of λ) and the quantity of interest λ'.

Here, we pursue an alternative approach, in which a water mass is instead directly defined based on an anomaly threshold λ' (Fig. 1b). The anomalous water mass is thus defined by:

$$\mathcal{M}_{\geq}(\lambda', t) = \int_{\Omega_{\geq}(\lambda', t)} \rho \, dV, \tag{6}$$

Applying the WMT framework to this anomalous water mass yields the familiar budget (Fig. 1b):

$$\frac{\partial}{\partial t}\mathcal{M}_{\geq}(\lambda') = \mathcal{S}_{\geq}(\lambda') + \Psi_{\geq}(\lambda') + \mathcal{G}_M(\lambda'), \tag{7}$$

which is analogous to the standard result, except that $\mathcal{G}_M(\lambda')$ depends on the material derivative of anomalies

$$\frac{D(\lambda')}{Dt} = \frac{\partial}{\partial t}(\lambda') + \mathbf{U} \cdot \nabla(\lambda'). \tag{8}$$

We emphasize that the transformation of these anomalous water masses (in tracer anomaly space) are an entirely distinct concept from the anomalous transformation of standard water masses (in tracer space).

As a proof of concept, we here evaluate budgets for anomalous water masses defined in terms of climatological anomalies of temperature. To introduce these concepts in a more accessible way before applying them to comprehensive ocean model output, we construct a synthetic temperature-like tracer field that evolves in space and time according to specified velocities and Eulerian temperature tendencies (Appendix B), complete with a seasonal cycle, a secular trend, and other variability modes (Figure B1). A major benefit of this analytical model is that it is not subject to any spurious numerical mixing or discretization errors, meaning we can be more confident in our calculations and interpretations of terms in the budgets. For example, Figure 2a shows the emergence of a water mass in the domain that is at least 2.93 (non-dimensional temperature units) warmer than the climatological mean, i.e. $\mathcal{M}_{\geq}(\Theta' = 2.93)$. The goal of the following sections is to derive a closed WMT budget that enables us to understand the processes driving this evolution.

c. Material evolution of temperature anomalies relative to a climatological seasonal cycle

Consider the conservative temperature Θ with the climatological seasonal cycle removed, i.e., the temperature anomaly Θ' relative to a climatological annual cycle $\overline{\Theta}$. To arrive at the anomalous

water mass budget, we begin from the generic tracer budget given by Eq. (9) and need to derive expressions for the material transformation terms, or tracer anomaly tendencies, that balance the kinematic material derivative $\frac{D(\Theta')}{Dt}$.

Subtracting the climatological mean equation [Eq. (10)] from the total temperature equation [Eq. (9)] yields the standard temperature anomaly tendency equation [Eq. (11)]:

$$\frac{\partial \Theta}{\partial t} = -\mathbf{U} \cdot \nabla \Theta + \dot{\Theta}, \tag{9}$$

$$\overline{\frac{\partial \Theta}{\partial t}} = -\overline{\mathbf{U}} \cdot \nabla \overline{\Theta} - \nabla \cdot \overline{\mathbf{U}'\Theta'} + \overline{\dot{\Theta}}, \tag{10}$$

$$\left(\frac{\partial \Theta}{\partial t}\right)' = -\mathbf{U} \cdot \nabla \Theta' - \nabla \cdot \left(\mathbf{U}'\overline{\Theta}\right) - \nabla \cdot \left(-\overline{\mathbf{U}'\Theta'}\right) + \dot{\Theta}', \tag{11}$$

where $\mathbf{U}$ denotes the velocity field, and $\dot{\Theta}$ represents the diabatic heat sources and sinks, including surface heat fluxes, geothermal heat fluxes, and mixing processes.

While Eq. (11) is often used to attribute the drivers of temperature variability encapsulated by the anomaly Θ', this approach implicitly assumes that the climatolical anomaly operation commutes with the time derivative, i.e. $(\partial_t \Theta)' = \partial_t(\Theta')$. This assumption breaks down when the climatological mean seasonal cycle is aperiodic, such that $\overline{\partial_t \Theta} \neq \partial_t \overline{\Theta}$, as in the presence of a significant mean warming, i.e. $\langle \partial_t \Theta \rangle > 0$, where the angle brackets denote a long-term (multi-year) average.

As a step towards an evolution equation for Θ', we define the detrended temperature $\tilde{\Theta} = \Theta - \langle \partial_t \Theta \rangle (t - t_0)$ by removing the integral of the mean tendency. As illustrated in Fig. B1d, this procedure ensures that $\overline{\partial_t \tilde{\Theta}} = \partial_t \overline{\tilde{\Theta}}$ for the detrended anomaly, enabling us to proceed with deriving an expression for the material tendency of temperature anomalies. Substituting the detrended anomaly into Eulerian tendency, we arrive at a revised budget equation for the detrended

temperature anomaly:

$$\frac{\partial \tilde{\Theta}}{\partial t} = -\mathbf{U}\cdot\nabla\Theta + \dot{\Theta} - \langle \partial_t \Theta \rangle, \tag{12}$$

$$\frac{\partial \overline{\tilde{\Theta}}}{\partial t} = -\overline{\mathbf{U}}\cdot\nabla\overline{\Theta} - \nabla\cdot(\overline{\mathbf{U}'\Theta'}) + \overline{\dot{\Theta}} - \langle \partial_t \Theta \rangle, \tag{13}$$

$$\frac{\partial \tilde{\Theta}'}{\partial t} = -\mathbf{U}\cdot\nabla\Theta' - \nabla\cdot\left(\mathbf{U}'\overline{\Theta}\right) - \nabla\cdot\left(-\overline{\mathbf{U}'\Theta'}\right) + (\dot{\Theta})', \tag{14}$$

Since the starting point for anomalous water mass transformation theory is an anomalous tracer conservation equation in the material form $\frac{\mathrm{D}\lambda'}{\mathrm{D}t} \equiv \frac{\partial \lambda'}{\partial t} + \mathbf{U}\cdot\nabla\lambda'$, Eq. (11) can be recast as a budget of the anomaly Θ':

$$\frac{\mathrm{D}\Theta'}{\mathrm{D}t} = \frac{\partial \Theta'}{\partial t} + \mathbf{U}\cdot\nabla\Theta' = (\dot{\Theta})' - \nabla\cdot\left(\mathbf{U}'\overline{\Theta}\right) - \nabla\cdot\left(-\overline{\mathbf{U}'\Theta'}\right) + \partial_t\left[(\langle \partial_t \Theta \rangle t)'\right]. \tag{15}$$

Meanwhile, Eq. (14) for the detrended anomaly is not yet in material form, because the material tendency involves the anomaly Θ', not the detrended anomaly. By partitioning the advective flux into components related to the long-team mean tendency anomaly and the detrended anomaly, the budget for the detrended anomaly $\tilde{\Theta}'$ can be expressed as:

$$\frac{\mathrm{D}\tilde{\Theta}'}{\mathrm{D}t} = \frac{\partial \tilde{\Theta}'}{\partial t} + \mathbf{U}\cdot\nabla\tilde{\Theta}' = (\dot{\Theta})' - \nabla\cdot\left(\mathbf{U}'\overline{\Theta}\right) - \nabla\cdot\left(-\overline{\mathbf{U}'\Theta'}\right) - \nabla\cdot(\mathbf{U}(\langle \partial_t \Theta \rangle t)'). \tag{16}$$

The last term on the RHS of Eq. (15) is non-zero due to the time-dependence of the climatological mean operator and represents how trends within the climatology estimation period get reflected into anomaly budgets (Figure B2c). This effect is mitigated by first detrending the anomalies, as evidenced by the absence of this term from the detrended budget [Eq. (16)]; however, the locally-detrended anomalies does not account for the advection of temperature anomalies associated with non-local trends, as revealed by the new last term on the right-hand side of Eq. (16).

The distinction between these two budget formulations is critical for practical applications under global warming scenarios. As demonstrated in Fig. 2a-b, the water mass of anomaly Θ' and detrended anomaly $\tilde{\Theta}'$ can be very different. Most notably, the tendency of Θ' retains the imprint

of long-term global warming, whereas the detrended anomaly isolates variability on all other timescales—excluding both the long-term mean tendency and the climatological seasonal cycle.

The tendency of Θ'- water mass displays characteristic step-like discontinuities at the juncture of successive annual cycles, a direct consequence of the persistent long-term mean tendency progressively shifting the climatological baseline. The detrended formulation, by contrast, preserves dynamical continuity; however, it remains influenced by the spatially heterogeneous long-term mean tendency, which modifies the detrended anomaly field through advection (the last term on the RHS of Eq. (16)) as shown in Fig. B2d. Given these different properties and budget structures, both anomaly definitions will be employed in the main text to develop their respective theoretical frameworks for anomalous water mass transformation.

d. Transformation budgets for anomalous water masses

The primary distinction between budgets for water mass $\mathcal{M}_{\geq}(\lambda)$ and anomalous water mass $\mathcal{M}_{\geq}(\lambda')$ is in transformation term $\mathcal{G}_M$. Combining Eq. (15) and Eq. (A6) yields the $\mathcal{G}_M$ of Θ'-water mass:

$$\begin{aligned}\mathcal{G}_M(\Theta') &= -\rho_0 \partial_{\Theta'} \int_{\Omega_{\geq} \cap R} \frac{\mathrm{D}\Theta'}{\mathrm{D}t}\, dV \\ &= -\rho_0 \partial_{\Theta'} \int_{\Omega_{\geq} \cap R} \left((\dot{\Theta})' - \nabla \cdot \left(\mathbf{U}' \overline{\Theta} \right) - \nabla \cdot \left(-\overline{\mathbf{U}'\Theta'} \right) + \partial_t \left[(\langle \partial_t \Theta \rangle t)' \right] \right) dV. \end{aligned} \tag{17}$$

Transformation of anomalous Θ'-water mass transformation thus consists of four components:

$$\mathcal{G}_M(\Theta') = \mathcal{G}_{\dot{\Theta}'} + \mathcal{G}_{U'\overline{\Theta}} + \mathcal{G}_{\overline{U'\Theta'}} + \mathcal{G}_{\langle \partial_t \Theta \rangle}. \tag{18}$$

The first term on the RHS is the transformation due to the anomalous material derivative of Θ', which corresponds directly to the WMT term in the standard analysis; the remaining three terms, however, have no equivalent in the standard WMT framework. The second term represents the contribution from the advection or stirring of velocity anomalies acting on the climatological temperature gradient, while the third term reflects how climatological heat fluxes due to correlations between temperature anomalies and velocity anomalies can transform anomalous water masses. The last term reflects the artificial transformation of anomalous water masses due to the aperiodic

nature of the climatogical seasonal cycle associated with a long-term mean warming. In practice, $\mathcal{G}_{\dot{\Theta}'}$ can be decomposed into contributions from anomalous surface heat flux, $\mathcal{G}_Q$, and anomalous mixing, $\mathcal{G}_{mix}$ (Fig. 1b).

Substituting Eq. (18) into Eq. (7) yields the Θ' water mass budget (Fig. 1b):

$$\frac{\partial}{\partial t}\mathcal{M}_{\geq}(\Theta') = \mathcal{S}_{\geq} + \Psi_{\geq} + \mathcal{G}_{\dot{\Theta}'} + \mathcal{G}_{U'\overline{\Theta}} + \mathcal{G}_{\overline{U'\Theta'}} + \mathcal{G}_{\langle\partial_t\Theta\rangle}. \tag{19}$$

We also investigate the water mass budget of the detrended anomaly, $\tilde{\Theta}'$ by combining Eq. (16) and Eq. (A6). Finally, the $\tilde{\Theta}'$-water volume budget is obtained by:

$$\mathcal{G}_M(\tilde{\Theta}') = -\rho_0\partial_{\tilde{\Theta}'}\int_{\Omega_{\geq}\cap R}\left((\dot{\Theta})' - \nabla\cdot\left(\mathbf{U}'\overline{\Theta}\right) - \nabla\cdot\left(-\overline{\mathbf{U}'\Theta'}\right) - \nabla\cdot\left(\mathbf{U}\left(\langle\partial_t\Theta\rangle\, t\right)'\right)\right)dV. \tag{20}$$

Here, the transformation term, $\mathcal{G}_M$ in $\tilde{\Theta}'$-water volume budget also includes four terms:

$$\mathcal{G}_M(\tilde{\Theta}') = \mathcal{G}_{\dot{\Theta}'} + \mathcal{G}_{U'\overline{\Theta}} + \mathcal{G}_{\overline{U'\Theta'}} + \mathcal{G}_{U(\langle\partial_t\Theta\rangle t)'} \tag{21}$$

Here the last term of RHS, $\mathcal{G}_{U(\langle\partial_t\Theta\rangle t)'}$, represents the contribution of spatial heterogeneity in temperature trends to water mass transformation of $\tilde{\Theta}'$.

Substituting Eq. (21) into Eq. (7) yields the $\tilde{\Theta}'$ water mass budget (Fig. 1b):

$$\frac{\partial}{\partial t}\mathcal{M}_{\geq}(\tilde{\Theta}') = \mathcal{S}_{\geq} + \Psi_{\geq} + \mathcal{G}_{\dot{\Theta}'} + \mathcal{G}_{U'\overline{\Theta}} + \mathcal{G}_{\overline{U'\Theta'}} + \mathcal{G}_{U(\langle\partial_t\Theta\rangle t)'}. \tag{22}$$

3. Application to an Analytical Model

To validate the anomalous water mass budget framework, we construct a dynamically consistent analytical model of temperature, $T = T(x,z,t)$, its Eulerian evolution, and the velocity field that advects it. This model serves as a rigorous testbed to verify temperature anomaly budget closure and further the anomalous water mass budget closure in Eqs. (A6). Ultimately, this analytical verification demonstrates the theoretical integrity of the proposed framework, facilitates a clear physical interpretation of each budget component, and provides a benchmark for evaluating potential sources of numerical error in discrete datasets. Anecdotally, the utility of this approach is

demonstrated by the fact that we only deciphered the subtle effects of mean trends on the anomalous WMT budget thanks to the analytical model, which in the case of ECCOv4r4 were relatively small and obscured by the non-closure of the WMT budget.

Figures 2a and 2b illustrate the time evolution of non-dimensional anomalous water mass defined by an extreme warm threshold, corresponding to the 95th percentile of the respective temperature anomalies. The discrepancy between the two time series reflects the differing definitions of the anomaly and the detrended anomaly. Under a persistent warming trend, the volume of the anomalous warm water mass increases substantially over time. In contrast, the detrended formulation isolates the interannual variability of extreme heat by removing both the seasonal cycle and the long-term mean tendency. The budgets close in both cases (Figs. 2c and 2d), with root-mean-square (RMS) residual errors of 6.8% and 6.3% relative to the RMS tendency for the Θ'- and $\tilde{\Theta}'$-based budgets, respectively. These small residuals demonstrate that the numerical implementation accurately captures the underlying closure of the anomalous water mass budget.

In this analytical case, we first examine the Θ'-WMT budget (Fig. 2c). The time tendency of the non-dimensional anomalous water mass is jointly regulated by diabatic processes ($\mathcal{G}_{\dot{\Theta}'}$), anomalous advection of the climatological temperature gradient ($\mathcal{G}_{U'\overline{\Theta}}$), and the climatological transient eddy flux ($\mathcal{G}_{\overline{U'\Theta'}}$). However, the annual tendency is dominated by pronounced "stair-step" discontinuities at each integer time, which arise from the reconstructed time mean tendency anomaly ($\mathcal{G}_{\langle\partial_t\Theta\rangle}$). As a result, the non-dimensional water mass tendency exhibits a systematic increase and enhanced variability.

We next consider the detrended budget (Fig. 2d), in which the influence of the time mean tendency anomaly is removed. In this case, the budget for the detrended extremely warm water mass is primarily governed by the competition between anomalous diabatic transformation ($\mathcal{G}_{\dot{\Theta}'}$) and the transformation associated with the spatial heterogeneity of the long-term mean tendency ($\mathcal{G}_{U(\langle\partial_t\Theta\rangle t)'}$). The contributions from anomalous advection ($\mathcal{G}_{U'\overline{\Theta}}$), climatological transient eddy fluxes ($\mathcal{G}_{\overline{U'\Theta'}}$), and boundary water mass flux (Ψ) are comparatively small, but remain necessary for accurate budget closure.

Figure 3 further quantifies the time-mean budget and its standard deviation across a full range of anomaly thresholds. The time-mean budget for the anomalous water mass (Figs. 3a and 3c) shows that closure is robustly maintained (Res ≈ 0) for the majority of intense warm and cold anomalies.

For the anomaly case (Fig. 3a), the non-dimensional mass change exhibits a pronounced positive tendency, primarily driven by the transformation associated with the long-term mean tendency anomaly ($\mathcal{G}_{\langle\partial_t\Theta\rangle}$). In contrast, for the detrended case (Fig. 3c), the net volume tendency is close to zero, reflecting the removal of the dominant low-frequency trend signal. The balance in this case is mainly governed by the offset between the transformation associated with the spatial heterogeneity of the long-term mean tendency and diabatic transformation.

The standard deviation of the budget terms (Figs. 3b and 3d) highlights the distinct temporal variability between the two cases. For the anomaly case (Fig. 3b), the variance is strongly amplified by the year-end discontinuities associated with the long-term mean tendency, leading to large fluctuations across thresholds. In contrast, the detrended case (Fig. 3d) exhibits reduced variability, with interannual fluctuations primarily governed by diabatic transformation and the transformation associated with the spatial heterogeneity of the long-term mean tendency. The increase in both the residual and its variability as the two anomaly threshold approaches zero does not indicate a theoretical inconsistency, but rather reflects numerical cancellation errors: at small thresholds, the budget involves differencing between large water mass volumes, rendering the discrete sampling more sensitive to rounding errors. These errors should not be misconstrued as spurious mixing – there isn't any in our analytical example.

In summary, the analytical application confirms the validity of the anomalous water mass budget theory. The anomalous Θ'-WMT framework successfully partitions water mass (or volume) changes into contributions from time mean tendency anomalies, advection of climatological gradients, climatological transient eddy fluxes, and diabatic transformation. Similarly, the detrended $\tilde{\Theta}'$-WMT framework accounts for the critical role of the spatial heterogeneity in the warming trend. Importantly, these two frameworks diagnose fundamentally different types of water mass anomalies. The Θ'-based budget captures variability that includes the influence of the long-term warming trend, while the $\tilde{\Theta}'$-based budget isolates variability relative to that trend. As a result, the inferred dominant processes and temporal evolution can differ substantially between the two formulations. One or the other may therefore be more appropriate depending on the scientific question being addressed. Together, these diagnostic terms, which are absent in standard WMT frameworks, provide a powerful new tool for deciphering the underlying dynamics of water mass variability in a changing climate.

4. Application to ECCOv4r4

The Estimating the Circulation and Climate of the Ocean (ECCO) version 4 release 4 (v4r4) state estimate serves as the primary dataset for our analysis. Unlike traditional atmospheric or oceanic reanalyses, ECCOv4r4 is derived through the adjoint method, ensuring a dynamically consistent and closed-budget representation of the ocean's state (Forget et al. 2015). This closure is particularly advantageous for water mass analysis, as it provides a comprehensive suite of diagnostic terms for the momentum, volume, and heat budgets, thereby eliminating the non-conservative increments that complicate budget-based studies in other reanalysis products. In this study, we utilize the daily output of ECCOv4r4 spanning 1 January 1993 to 30 December 2017 to diagnose the anomalous water masses budget of temperature.

Figure 4a shows the time evolution of the global water mass defined by the anomaly (Θ') exceeding 3.5°C. This threshold is chosen to represent extremely anomalous water masses, with other threshold choices shown in Fig. 6. The resulting time series exhibits two prominent peaks: the largest occurring in late 1997 to early 1998, and the second largest in late 2015 to early 2016. These peaks coincide with the two most intense El Niño events on record (Trenberth 1997; McPhaden 1999; Santoso et al. 2017). Consistent with this correspondence, the global anomalous water mass is moderately correlated with the Niño3.4 index ($r \approx 0.58$). A similar correlation is obtained for the detrended anomaly, indicating that this relationship reflects interannual variability rather than a shared long-term trend.

In addition, some of the smaller peaks in the time series may be associated with La Niña conditions (negative phases of the Niño3.4 index). Given that the $\Theta' > 3.5$°C water mass is primarily concentrated in the tropical Pacific and Indian Oceans, this behavior may reflect a redistribution of heat between ocean basins across different phases of ENSO (not shown). The time series of the warm water mass defined by the detrended anomaly ($\tilde{\Theta}'$, Fig. 4b) exhibits only a slight difference in magnitude compared to that based on Θ'. This contrasts with the analytical case (Figs. 2a,b), and can be attributed to the relatively modest warming trends in the real ocean compared to the idealized scenario.

Figures 4c and d show the Θ'-water mass budget framework applied to ECCOv4r4 [Eq. (C29)], integrated in time to facilitate comparison to the anomalous water mass timeseries. The warm water budget reveals that the net increase of this warm water mass is dominated by the water mass

transformation due to anomalous velocity advecting the climatological temperature ($\mathcal{G}_{U'\overline{\Theta}}$), while interior diabatic mixing constitutes the primary contribution to water mass destruction, followed by the climatological transient eddy heat flux ($\mathcal{G}_{\overline{U'\Theta'}}$). Notably, anomalous surface heat flux also acts to erode the warm water mass, but this contribution is almost exclusively concentrated during the two super El Niño events. Finally, the climatological transient eddy heat flux is relatively small, comparable in magnitude to the residual, which encompasses errors linked to discretization in temperature space, numerical errors that may or may not be interpreted as spurious mixing (Megann 2018; Bailey et al. 2023), and other unresolved processes.

Figure 5 shows the corresponding WMT budget, which is simply the time derivative of the warm water budgets shown in Figure 4. The residual is negligibly small at all times, confirming the validity of both our theoretical framework and numerical implementation, and indicating that the well-resolved dynamical terms provide valuable insights into the variability of the global warm water mass. The most prominent feature is that this variability is dominated by the advection of climatological temperature by velocity anomalies (orange line). During the two extreme El Niño events of 1997/98 and 2015/16, this anomalous advection could be the eastward transport of warm water from the western Pacific warm pool, leading to the accumulation of the global warm water mass (McPhaden 1999; Santoso et al. 2017). This is consistent with the classical Bjerknes feedback mechanism, in which anomalous westerly winds drive anomalous oceanic advection, further amplifying the warm sea surface temperature anomalies (Capotondi et al. 2015). Notably, the surface heat flux anomaly (red line) acts as a heat sink throughout nearly the entire duration of both events, including during their growth phases, reflecting the enhanced ocean-to-atmosphere heat release that characterizes extreme El Niño events (Trenberth 1997; Santoso et al. 2017). The $\tilde{\Theta}'$-water mass budget (Eq. C34; Figure 5b) exhibits a pattern largely similar to that of the Θ'-water mass budget, consistent with the negligible difference in warm water mass volume between the two definitions. Overall, these results highlight the potential of our framework to capture the full life cycle of anomalous warm water mass variability, and motivate future investigations into the regional contributions and dynamical origins of such signals.

Figure 6 further shows the time-averaged anomalous water mass budget and the corresponding standard deviations across a range of temperature anomaly thresholds. Both the Θ'- and $\tilde{\Theta}'$-water mass budgets achieve good closure at relatively large warm or cold temperature anomalies. The

residual increases as the temperature anomaly approaches zero, consistent with the analytical case (figure 3), and attributable to numerical errors arising from the computation of small differences between two large water mass volumes, which makes the discrete sampling framework more sensitive to rounding and differencing errors.

Beyond the closure behavior, the budget patterns reveal that the tendency of the water mass at extreme temperature anomalies is primarily dominated by the advection of climatological temperature by velocity anomalies (orange lines), whereas at moderate temperature anomalies, the tendency reflects a balance among mixing anomalies (blue lines), surface heat flux anomalies (red lines), and the advection of climatological temperature by velocity anomalies (orange lines). Regarding the variability of the budget terms, the standard deviations indicate that the rates of change are dominated by the advection of climatological temperature by velocity anomalies across most temperature anomaly thresholds. This highlights the short-timescale activity of each process, even when their time-mean contributions are small.

In summary, the application of the anomalous water mass budget framework to ECCOv4r4 demonstrates its ability to accurately close the mass budget of globally defined anomalously warm and cold water masses, while providing a dynamically consistent decomposition of the processes governing their variability. The framework reveals that anomalous oceanic advection is the primary driver of variability of extremely warm water masses, particularly during the two most intense El Niño events of the satellite era, whereas surface heat flux anomalies and mixing consistently play a damping role. These results establish the robustness of the framework as a powerful diagnostic tool and motivate its further application to regional water mass analyses and the investigation of other climate phenomena.

5. Conclusions

In this study, we have developed a novel theoretical framework for the budget of anomalous water masses, in which water masses are defined by bounds on tracer anomalies rather than absolute tracer values. To our knowledge, this represents the first systematic derivation of a transformation budget for anomalous water masses, extending the classical Water Mass Transformation (WMT) theory to the space of climatological anomalies. The key theoretical contribution is the derivation of the material tendency of tracer anomalies, which introduces three additional transformation

terms absent from the standard WMT framework: the contribution from time mean tendency, the advection of climatological tracer gradients by velocity anomalies, and the climatological-mean eddy heat flux. We further distinguish between two anomaly definitions — the anomaly Θ' and the detrended anomaly $\tilde{\Theta}'$ — and derive their respective budget equations, demonstrating that the choice of anomaly definition has important implications for the interpretation of water mass variability under a long-term warming trend, although these additional corrections appear to be relatively small in context of real ocean warming rate.

The framework was first validated against an analytical model, which confirmed budget closure and provided a clear physical interpretation of each transformation term. The analytical case demonstrated that the detrended formulation effectively isolates interannual variability by removing both the seasonal cycle and the long-term mean tendency, while the anomaly framework retains the imprint of global warming. Both formulations achieve robust budget closure, with residuals remaining negligible across a broad range of anomaly thresholds, with the exception of near-zero thresholds where numerical cancellation errors become significant.

The framework was then applied to the ECCOv4r4 ocean state estimate to diagnose the budget of global anomalous warm water masses over the period 1993–2017. The global warm water mass defined by temperature anomalies exceeding 3.5°C exhibits two prominent peaks coinciding with the two most intense El Niño events on record — the 1997/98 and 2015/16 events — consistent with the anomalously warm sea surface temperatures in the tropical Pacific during these periods. Budget analysis reveals that anomalous advection of the climatological temperature gradient by velocity anomalies is the dominant driver of warm water mass variability, particularly during extreme El Niño events, consistent with the classical Bjerknes feedback mechanism. In contrast, surface heat flux anomalies act as a consistent heat sink throughout both events, reflecting enhanced ocean-to-atmosphere heat release. The negligibly small residuals confirm the validity and numerical consistency of the framework when applied to a dynamically consistent ocean state estimate.

These results establish the anomalous water mass budget framework as a powerful diagnostic tool for characterizing the life cycle of ocean anomalies associated with climate variability and extreme events. Future work should extend this framework to regional water mass analyses, explore its application to other tracers anomalies of interest, and investigate the regional contributions to the global anomalous warm water mass variability identified here.

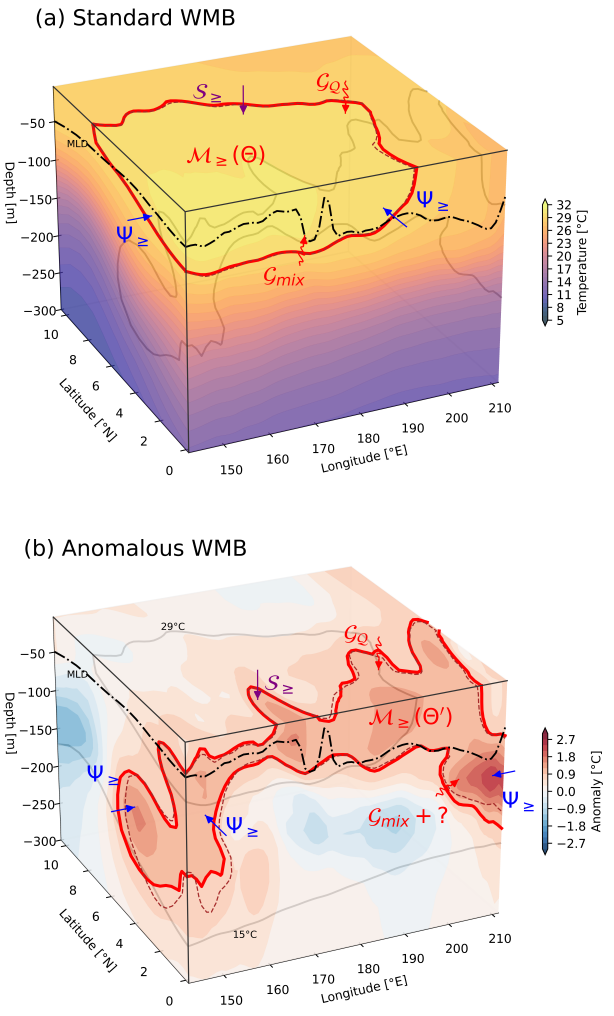

FIG. 1. (a) Color shading shows sea temperature from ECCOv4r4 on 1 January 2015. The red contour marks the 29°C isotherm, enclosing the water mass with $\Theta > 29$°C. The brown contour shows the 29°C isotherm on 2 January 2015, indicating its evolution. The black dot–dashed line denotes the daily mean mixed layer depth (MLD) on 1 January 2015. Light gray contours show the 0.9°C positive temperature anomaly on 1 January 2015. This panel illustrates the geometric definition and temporal evolution of water masses used in the standard water mass budget [Eq. (2)]. The transformation term $\mathcal{G}_{\dot{\Theta}}$ is decomposed into surface heat flux and mixing contributions, $\mathcal{G}_Q$ and $\mathcal{G}_{\mathrm{mix}}$, respectively, following Eq. (C29). (b) Color shading shows the temperature anomaly on 1 January 2015. The red contour marks the 0.9°C anomaly, enclosing the water mass with $\Theta' > 0.9$°C. The brown contour shows the 0.9°C anomaly on 2 January 2015. The black dot–dashed line denotes the daily mean MLD on 1 January 2015. Light gray contours show the 29°C isotherm. This panel illustrates the geometric framework for anomalous water masses used in the anomalous water mass budget [Eq. (7)]. In this case, the transformation term $\mathcal{G}_{\dot{\Theta}}$ includes additional contributions beyond $\mathcal{G}_Q$ and $\mathcal{G}_{mix}$, as defined in Eq. (C29), reflecting the modified transformation processes in the anomalous framework.

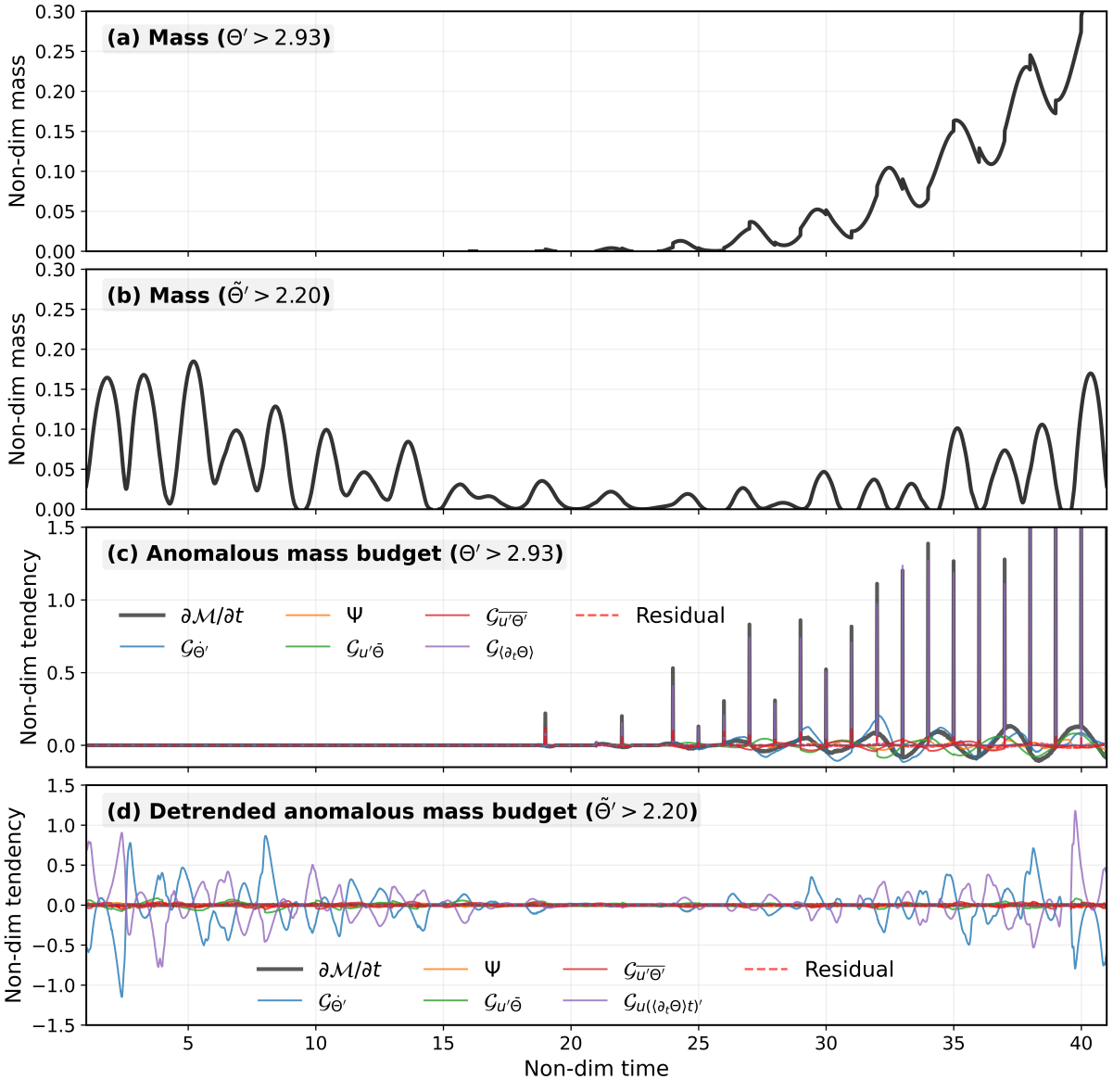

FIG. 2. (a) Time evolution of the non-dimensional water mass defined by the anomaly (Θ') warmer than the 95th percentile threshold (2.93). (b) As in (a), but for the detrended anomaly ($\tilde{\Theta}'$) exceeding its 95th percentile threshold (2.20). (c) Time series of individual budget components from the anomalous budget [Eq. (19)] for the 95th percentile anomalous water mass defined by Θ'. The budget is evaluated using a finite time interval Δt (here $\Delta t = 0.01$ yr), and thus the magnitude of the "stair-step" discontinuities reflects this temporal discretization. In particular, shorter Δt would lead to larger instantaneous tendencies, while longer Δt smooths these variations without altering the underlying budget closure. (d) As in (c), but for the detrended anomaly using the detrended anomalous budget [Eq. (22)]. All budget terms are shown except $\mathcal{S}$, as there is no surface mass flux in the analytical case.

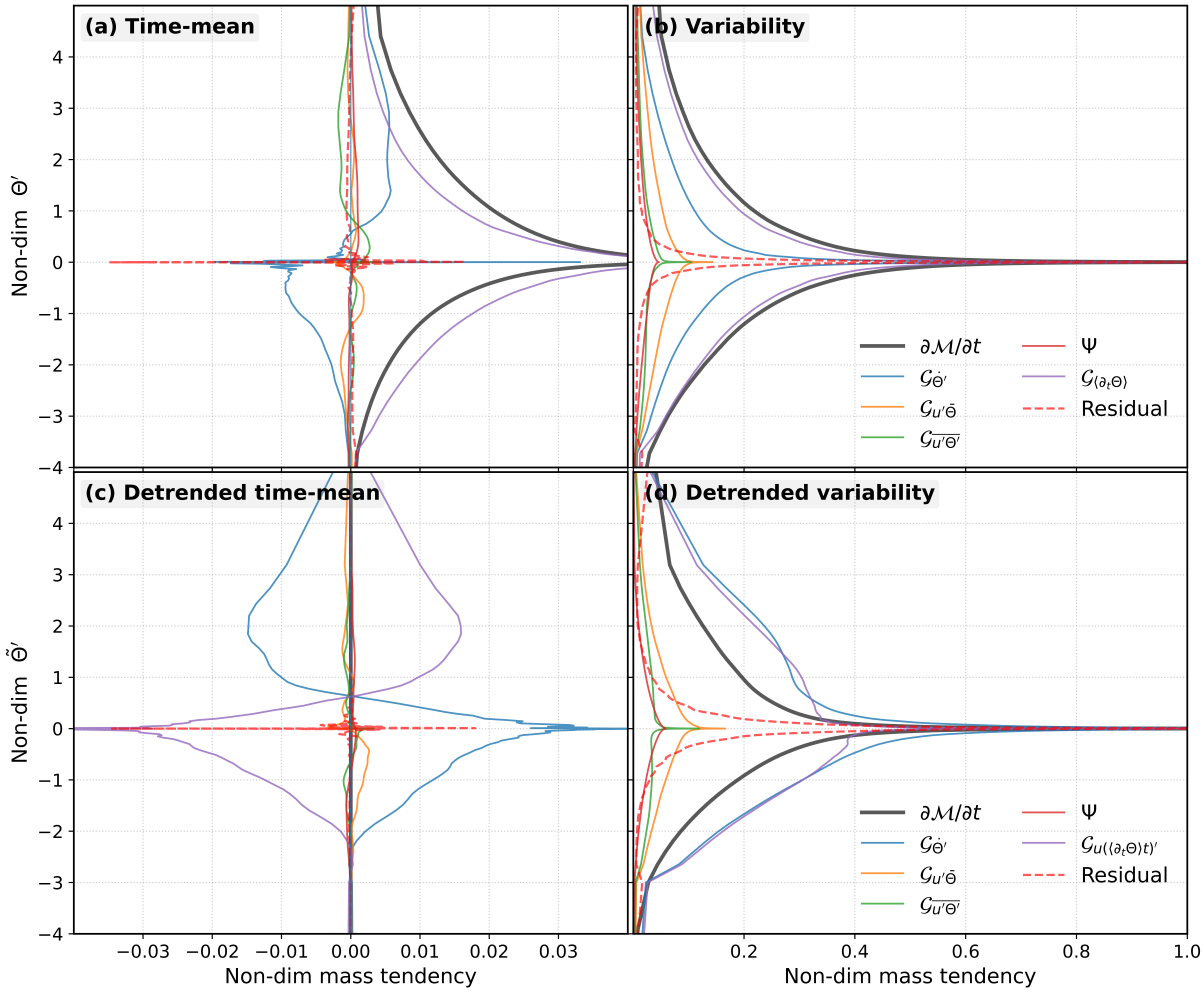

FIG. 3. Statistical analysis of the non-dimentional anomalous water mass budget as a function of temperature anomaly thresholds. (a) Time-averaged budgetary components for the anomaly (Θ') across a range of temperature thresholds. (b) Corresponding standard variance of budgetary components for the anomaly (Θ'). (c, d) As in (a, b), but for the detrended anomaly ($\tilde{\Theta}'$) budget and its standard variance.

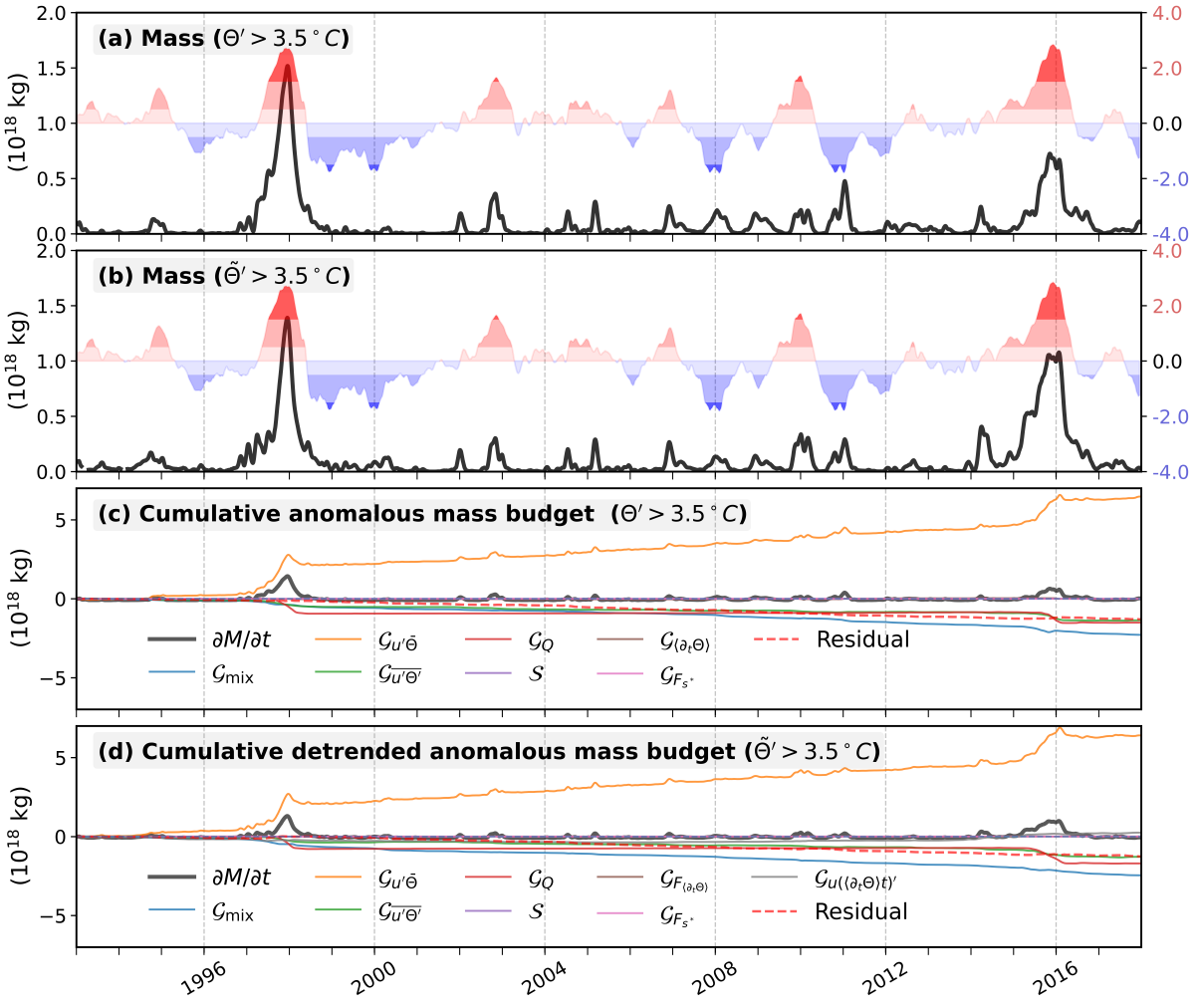

FIG. 4. (a) Daily time evolution of the global water mass defined by the anomaly (Θ') exceeding 3.5ºC spanning 1 January 1993 to 30 December 2017 in ECCOv4r4. The Niño3.4 index derived from ECCOv4r4 is overlaid (right axis) using a 30-day moving average. El Niño (La Niña) conditions are indicated by red (blue) shading when Niño3.4 exceeds ±0.5°C, with darker shading for anomalies exceeding 1.5°C. (b) As in (a) but for the detrended anomaly ($\tilde{\Theta}'$) exceeding 3.5ºC. (c) Time series of individual cumulative budgetary components (within the anomalous budget – Eq. (C29)) for the global water mass defined by the anomaly (Θ') exceeding 3.5ºC. (d) As in (c) but for the detrended anomalous budget [Eq. (C34)]. All time series have been smoothed with a 30-day moving average.

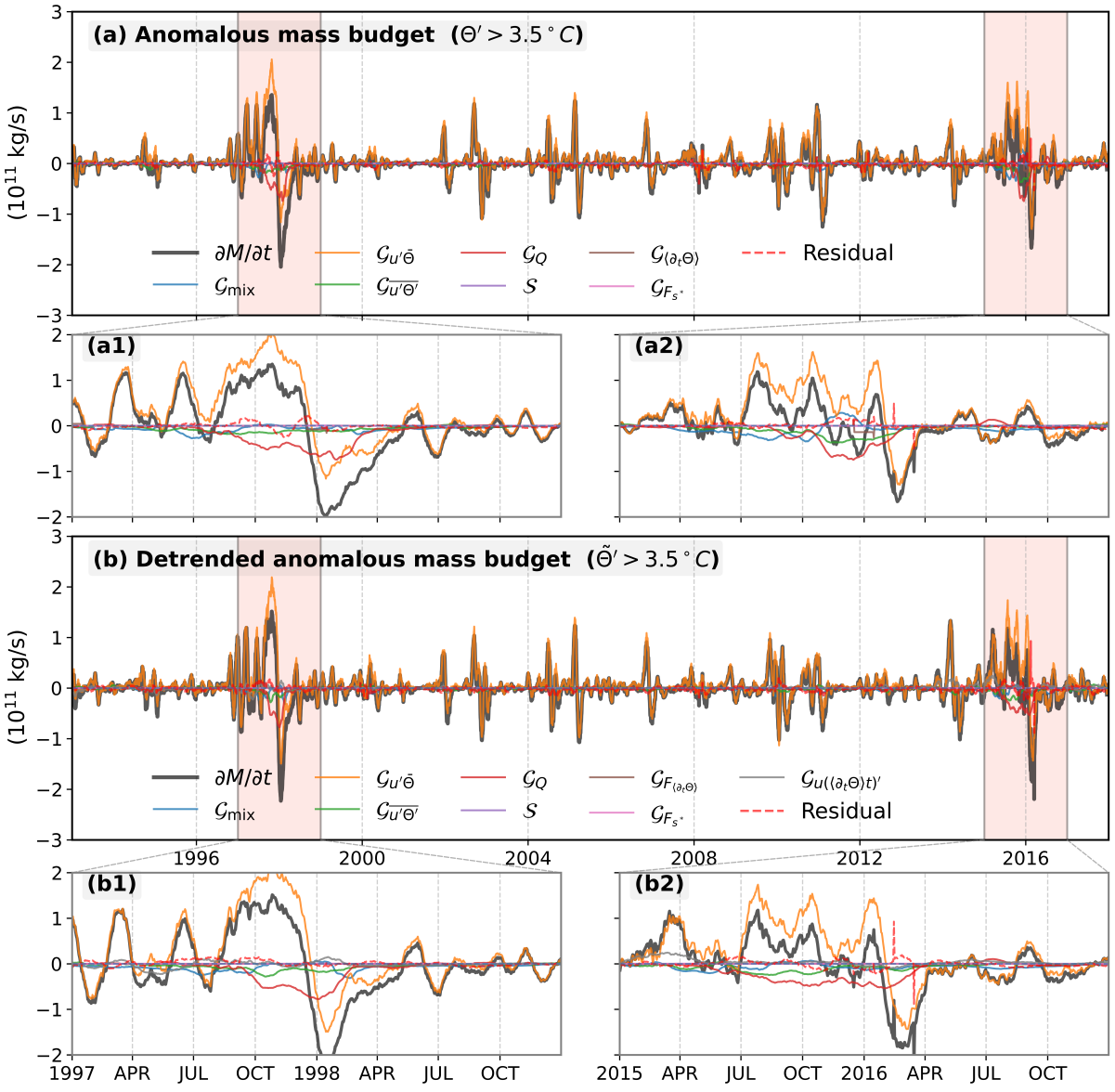

FIG. 5. (a) Time series of individual budget terms from the anomalous water mass budget [Eq. (C29)] for the global water mass defined by full temperature anomalies exceeding $\Theta' > 3.5$°C. Panels (a1) and (a2) show zoomed-in views of (a) for the periods 1997 January 1 – 1998 December 31 and 2015 January 1 – 2016 December 31, respectively. (b) As in (a), but for the detrended anomaly water mass budget [Eq. (C34)]. Panels (b1) and (b2) show the corresponding zoomed-in views for the detrended anomaly. All time series have been smoothed with a 30-day moving average.

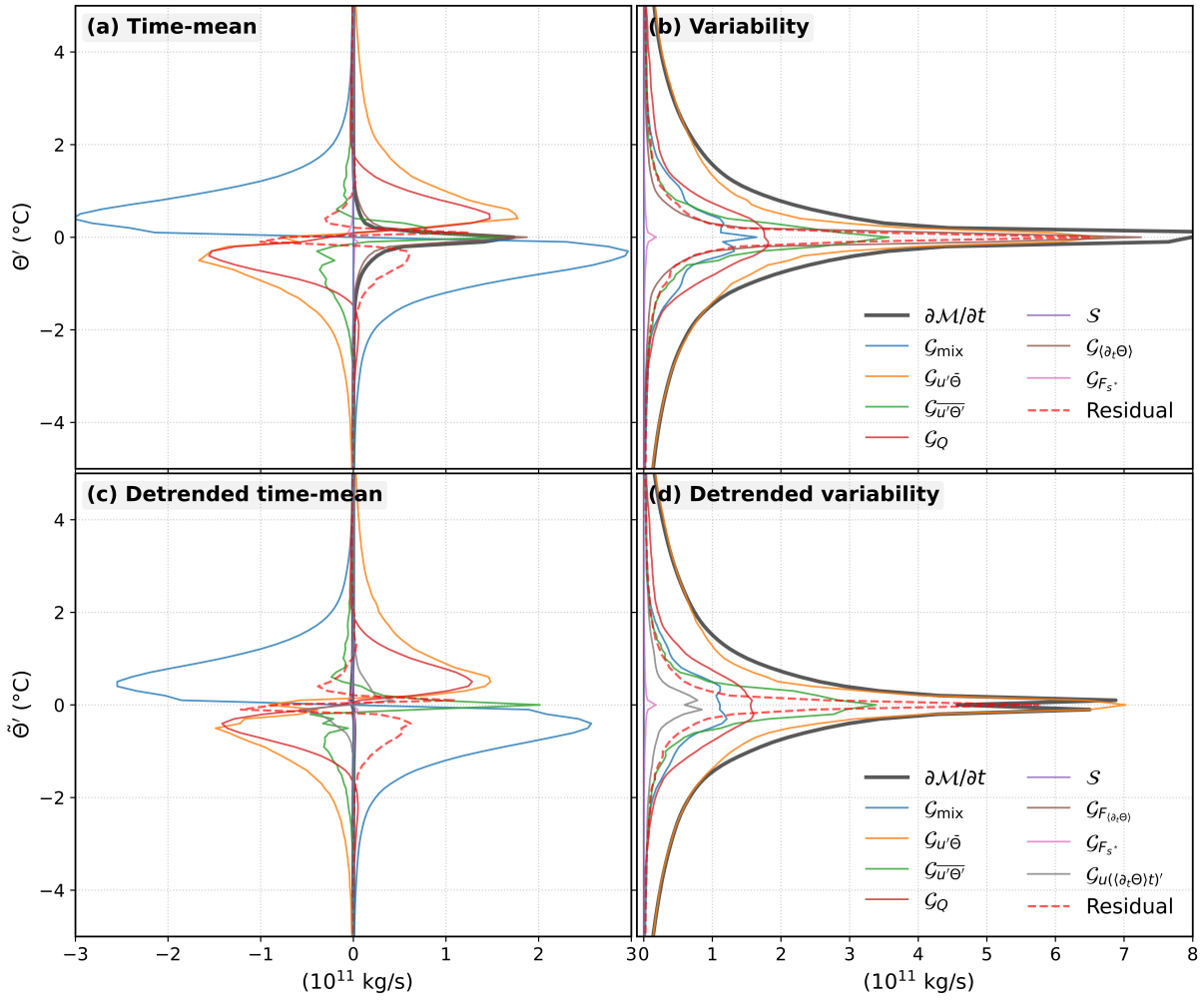

397 FIG. 6. Statistical analysis of the global anomalous water mass budget as a function of temperature anomaly
398 thresholds in ECCOv4r4. (a) Time-averaged budgetary components for the anomaly (Θ') across a range of
399 temperature thresholds. (b) Corresponding standard variance of budgetary components for the anomaly (Θ'). (c,
400 d) As in (a, b), but for the anomaly ($\tilde{\Theta}'$) budget and its standard variance.

Acknowledgments. This research is funded by the Gordon and Betty Moore Foundation through Grant GBMF13919 to UCI to support the work of Ran Liu. Additional support was provided by NASA and NOAA through their respective grant programs.

Data Availability Statement

The ECCO Version 4 Release 4 (ECCOv4r4) daily average and snapshot products used in this study are publicly available through the NASA Physical Oceanography Distributed Active Archive Center (PO.DAAC) at `https://podaac.jpl.nasa.gov/ECCO`.

APPENDIX A

Derivation of the Boussinesq Water Mass Transformation budget from first principles

Applying the Leibniz-Reynolds transport theorem to the time derivative of the water mass $\mathcal{M}_{\geq}$ defined in Equation 1, we find that the time tendency of the water mass arises from two contributions–changes in density (within a fixed volume) and changes in volume:

$$\frac{\partial}{\partial t}\mathcal{M}_{\geq}(\lambda,t) = \int_{\Omega_{\geq}(\lambda,t)} \frac{\partial \rho}{\partial t}\, dV + \oint_{\partial\Omega_{\geq}(\lambda,t)} \rho\, \mathbf{U}^{(\partial\Omega_{\geq})} \cdot \hat{\mathbf{n}}\, dS. \tag{A1}$$

Here $\partial\Omega_{\geq}(\lambda,t)$ denotes the boundary of the water mass, and $\mathbf{U}^{(\partial\Omega_{\geq})}$ represents the instantaneous velocity of this moving boundary–distinct from the fluid velocity $\mathbf{U}$.

Under the Boussinesq approximation—commonly adopted in ocean models—the fluid is assumed nearly incompressible, such that ρ is treated as a constant ρ_0 in Eq. (A1). Under this approximation, the water mass $\mathcal{M}_{\geq}$ enclosed by a body of water $\Omega_{\geq}(\lambda,t)$ is simply proportional to the enclosed volume of water $\mathcal{V}_{\geq} \equiv \int_{\Omega_{\geq}(\lambda,t)} dV = \mathcal{M}_{\geq}/\rho_0$. While this approximation motivates some authors to express water mass transformations in units of volume, we find it more generalizable and natural–given the terminology–to work directly in terms of mass, even in the Boussinesq applications that follow.

While the first term on the RHS of Eq. (A1) vanishes under the Boussinesq approximation, it will prove useful to nevertheless substitute the mass conservation equation, $\partial_t \rho = -\nabla \cdot (\rho \mathbf{U})$, to make the flow divergence appear explicitly, revealing that water mass change arises due to the competition between flow through the water mass' boundary and the movement of the boundary

itself through the water:

$$\frac{\partial}{\partial t}\mathcal{M}_{\geq}(\lambda,t) = -\rho_0 \oint_{\partial\Omega_{\geq}(\lambda,t)} \left(\mathbf{U} - \mathbf{U}^{(\partial\Omega_{\geq})}\right) \cdot \hat{\mathbf{n}}\, dS, \tag{A2}$$

Walin's (1977) insight is to separately consider the contributions to the surface integral in from different types of boundaries. We introduce the notation $\partial\Omega_{\geq}(t) = (\partial\Omega_{\geq}(t) \cap R) \cup (\Omega_{\geq}(t) \cap \partial R)$ to distinguish the physical boundaries of the water mass within the region (the first term) from the artificial boundaries that arise by confined the water mass to a region of interest R (the second term). A useful decomposition is then:

$$0 = \oint_{\partial\Omega_{\geq}} \mathbf{U} \cdot \hat{\mathbf{n}}^{(\partial\Omega_{\geq})}\, dS = \int_{\partial\Omega_{\geq}^{\text{surf}} \cap \partial R} \mathbf{U} \cdot \hat{\mathbf{n}}^{(\text{surf})}\, dS + \int_{\Omega_{\geq} \cap \partial R} \mathbf{U} \cdot \hat{\mathbf{n}}^{(\partial R)}\, dS + \partial_\lambda \int_{\Omega_{\geq} \cap R} \mathbf{U} \cdot \nabla\lambda\, dV. \tag{A3}$$

Here, the first term on the RHS represents the volume flux across the surface boundary; the second, the flux across the lateral region boundary; and the third, the flux across the λ tracer isosurface, which we rewrite using the standard transformation relationship. We assume there is no mass flux across the seafloor.

Before deriving the contribution of instantaneous volume change to the water mass tendency, we recall a purely kinematic identity associated with the evolving tracer isosurface. Along an isosurface of the tracer λ, the total derivative of λ vanishes identically, since the surface is defined by the level-set condition $\lambda(x,t) = \text{const}$. Specifically,

$$\frac{d\lambda}{dt} = \frac{\partial\lambda}{\partial t} + \mathbf{U}^{(\partial\Omega_{\geq})} \cdot \nabla\lambda = 0, \qquad \text{along the } \lambda\text{-isosurface .} \tag{A4}$$

This statement is purely kinematic and therefore remains valid even when λ represents a tracer anomaly. The interface velocity $\mathbf{U}^{(\partial\Omega_{\geq})}$ corresponds to the full velocity field that advects the surface, rather than to any anomalous component. This kinematic constraint forms the basis for the consistent formulation of the anomalous water mass budget developed below.

Then applying Eq. (A4) to the second term of Eq. (A1) and noting that the diatracer unit vector is defined by $\hat{\mathbf{n}}^{(\lambda)} = \nabla\lambda/|\nabla\lambda|$, the contribution from the instantaneous volume change can be rewritten

as:

$$\begin{aligned}
\oint_{\partial\Omega_{\geq}\cap R} \mathbf{U}^{(\partial\Omega_{\geq})}\cdot\hat{\mathbf{n}}\,dS &= \int_{\partial\Omega_{\geq}^{\mathrm{surf}}\cap\partial R} \mathbf{U}^{(\mathrm{surf})}\cdot\hat{\mathbf{n}}^{(\mathrm{surf})}\,dS + \oint_{\partial\Omega_{\geq}\cap R} \frac{\mathbf{U}^{(\partial\Omega_{\geq})}\cdot\nabla\lambda}{|\nabla\lambda|}\,dS \\
&= \int_{\partial\Omega_{\geq}^{\mathrm{surf}}\cap\partial R} \mathbf{U}^{(\mathrm{surf})}\cdot\hat{\mathbf{n}}^{(\mathrm{surf})}\,dS + \oint_{\partial\Omega_{\geq}\cap R} \left(-\frac{\partial\lambda}{\partial t}\right)\frac{1}{|\nabla\lambda|}\,dS \\
&= \int_{\partial\Omega_{\geq}^{\mathrm{surf}}\cap\partial R} \mathbf{U}^{(\mathrm{surf})}\cdot\hat{\mathbf{n}}^{(\mathrm{surf})}\,dS - \partial_{\lambda}\int_{\Omega_{\geq}\cap R}\frac{\partial\lambda}{\partial t}\,dV. \qquad \text{(A5)}
\end{aligned}$$

Here the first term on the RHS represents the contribution from the surface (or bottom) boundary to the volume change, while the second term reflects the effect of the tracer tendency—the water mass transformation term.

Further, combining Eqs. (A3) and (A5) and multiplying by ρ_0 yields the λ-water mass budget:

$$\begin{aligned}
\frac{\partial}{\partial t}\mathcal{M}_{\geq}(\lambda,t) &= -\rho_0\int_{\partial\Omega_{\geq}^{\mathrm{surf}}\cap\partial R}\left(\mathbf{U}-\mathbf{U}^{(\mathrm{surf})}\right)\cdot\hat{\mathbf{n}}^{(\mathrm{surf})}\,dS \\
&\quad -\rho_0\int_{\Omega_{\geq}\cap\partial R}\mathbf{U}\cdot\hat{\mathbf{n}}^{(\partial R)}\,dS \\
&\quad -\rho_0\partial_{\lambda}\int_{\Omega_{\geq}\cap R}\left(\frac{\partial\lambda}{\partial t}+\mathbf{U}\cdot\nabla\lambda\right)dV. \qquad \text{(A6)}
\end{aligned}$$

For any tracer λ, Eq. (A6) shows that the tendency of the λ-classified water mass within a region R can be decomposed into three terms:

1. surface mass exchanges $\mathcal{S}_{\geq}$ (so small it is neglected in most contexts),
2. lateral boundary transport $\Psi_{\geq}$ (which vanishes if the region R completely encloses the body of water, as in global analyses), and
3. cross-isosurface transformation $\mathcal{G}_M$, controlled by the material derivative $\frac{D\lambda}{Dt}=\frac{\partial\lambda}{\partial t}+\mathbf{U}\cdot\nabla\lambda=\dot{\lambda}$.

Therefore, the key to deriving any closed water mass budget is to determine the processes that contribute to the tracer's material tendency.

APPENDIX B

Analytical Temperature Model and Discretization of the Budget Calculations

a. Model Configuration and Discretization

For an initial test of the anomalous water mass framework, we construct an idealized analytical model of non-dimensional temperature variability. The horizontal domain spans a dimensionless range $x \in [0,3]$, discretized with a uniform spacing $\Delta x = 0.0035$ ($N_x = 858$). $\Delta y = 1$ ($N_y = 1$). The reference density (ρ_0) is set to 1 for simplicity. The temporal domain covers $t \in [1,41]$, where $t = 1$ defines one model "year", corresponding to the primary "seasonal cycle" frequency $\Omega_1 = 2\pi$. High-frequency variability is resolved using a sampling rate of $\Delta t = 0.01$ (100 samples per year).

Reflecting the architecture of modern General Circulation Models (GCMs), the vertical grid employs exponential stretching to enhance resolution in the upper ocean. The physical depth $z \in [0,4000]$ m is mapped to a computational coordinate $\eta \in [0,1]$ via the cumulative depth function:

$$z_c(\eta) = \frac{e^{\alpha\eta} - 1}{e^{\alpha} - 1} \cdot z_{\max}, \tag{B1}$$

where $\alpha = 3$ is the stretching parameter. Discrete cell centers z_k are located at the midpoints of the layers: $z_k = (z_{c,k} + z_{c,k-1})/(2z_{\max})$. This configuration yields 50 vertical levels concentrated near the surface to capture intensified velocity profiles and sharp thermal gradients. All spatiotemporal coordinates are treated as dimensionless.

b. Governing Equations and Analytical Gradients

The instantaneous temperature field $\Theta(x,z,t)$ is constructed as the product of a horizontal field with a vertical structure function $f(z)$:

$$\Theta(x,z,t) = [\Theta_{\text{wave}}(x,t) + \Theta_{\text{back}}(x) + \Theta_{\text{trend}}(x,t) + c]\, f(z), \tag{B2}$$

where $f(z) = 1 - \tanh[(z - H_1)/\delta]$. The transient component Θ_{wave} represents seasonal oscillations and propagating wave modes:

$$\Theta_{\text{wave}}(x,t) = \sum_{i=1}^{2} a_i \cos(\Omega_i t) + a_3 \sin[k_1(x - c_p t)] + a_4 \sin[k_2(x - c_p t)]. \tag{B3}$$

The background state, $\Theta_{\text{back}}(x) = \gamma x$, prescribes a constant horizontal temperature gradient to mimic zonal sea surface temperature (SST) transitions. To simulate complex climate signals,

Θ_{trend} incorporates an accelerating warming trend and periodic interannual variability:

$$\Theta_{\text{trend}}(x,t) = \underbrace{[b_{\text{linear}} + b_{x,\text{amp}}\cos(k_x x)]t}_{\text{Spatially-modulated warming trend}} + \underbrace{b_{\text{accel}}t^2}_{\text{Acceleration}} + \underbrace{a_{\text{low}}\sin(\Omega_{\text{low}}t + \phi_{\text{low}})}_{\text{Interannual variability mode}}, \tag{B4}$$

where $b_{x,\text{amp}}$ introduces spatial heterogeneity in the warming rate. Fig. B1a shows a snapshot of the analytical temperature.

The velocity field $u(z,t)$ is surface-intensified and oscillatory:

$$u(z,t) = u_0[1 + a_5\sin(\Omega_3 t)] \cdot \exp(-z/H_2). \tag{B5}$$

The velocity is spatially uniform ($\partial u/\partial x = 0$), ensuring mass conservation ($\nabla \cdot \mathbf{u} = 0$) with zero vertical velocity ($w = 0$).

The local tendency $\partial\Theta/\partial t$ and horizontal gradient $\partial\Theta/\partial x$ are derived analytically to ensure the governing equations are satisfied exactly:

$$\frac{\partial\Theta}{\partial t} = f(z)\left[-\sum_{i=1}^{2} a_i\Omega_i\sin(\Omega_i t) - \sum_{j=1}^{2} a_{j+2}k_j c_p\cos\phi_j + \frac{\partial\Theta_{\text{trend}}}{\partial t}\right], \tag{B6}$$

$$\frac{\partial\Theta}{\partial x} = f(z)\left[\sum_{j=1}^{2} a_{j+2}k_j\cos\phi_j - b_{x,\text{amp}}k_x\sin(k_x x)t + \gamma\right], \tag{B7}$$

where $\phi_j = k_j(x - c_p t)$. The diabatic forcing implied by these tendencies is then derived analytically in closed-form: $\dot{\Theta} = \partial_t\Theta + u\partial_x\Theta$. This analytical formulation provides a "ground truth" benchmark for budget verification. All parameters assigned to these analytical expressions are summarized in Table B1. It should be emphasized that while the parameters are specifically chosen to mimic the multi-scale complexity of observed oceanic temperature variability, they do not affect the fundamental closure of the budget. Rather, achieving exact closure under such intricate spatiotemporal conditions further demonstrates the robustness and theoretical rigor of the proposed framework. A major advantage of this analytical approach is that water mass budgets can be exactly closed, as there are no discretization errors; by contrast, water mass budgets in finite-volume GCMs exhibit significant amounts of spurious mixing, which appear as a residual term when attempting to close water mass budgets (Griffies et al. 2000; Lee et al. 2002; Drake et al. 2025).

TABLE B1. Parameters for the non-dimensional analytical model configuration.

Parameter	Value	Parameter	Value
a_1, a_2 (Seasonal)	1.0, 0.5	b_{linear} (Linear trend)	0.04
a_3, a_4 (Waves)	2.0, 1.0	b_{accel} (Accel. trend)	0.003
a_5 (Velocity osc.)	4.5	$b_{x,\text{amp}}$ (Trend mod.)	0.04
k_1, k_2	$17.5\pi/x_{\max}, 0.25k_1$	k_x (Trend mod. k)	$1.5 \cdot 2\pi/x_{\max}$
Ω_1, Ω_2	$2\pi, 2\pi/2.7$	$a_{\text{low}}, \Omega_{\text{low}}$	$0.4, 2\pi/50$
Ω_3 (Vel. freq)	$2\pi/3$	ϕ_{low}, c	0, 15.0
u_0 (Ref. velocity)	0.08	γ (Back. gradient)	-3.0
c_p (Phase speed)	0.5	H_1, H_2, δ (Vertical)	0.025, 0.05, 0.25

c. Time-averaged Diagnostics and Budget Closure

To mimic the way GCM budget diagnostics are archived, we compute time-averaged fields χ_{avg} over intervals of $\Delta t = 0.01$ using analytical antiderivative functions $\mathcal{I}_\chi \equiv \int \chi \, \mathrm{d}t$:

$$\chi_{\text{avg}} = \frac{\mathcal{I}_\chi(t + \Delta t) - \mathcal{I}_\chi(t)}{\Delta t}, \quad \chi \in \{\Theta, u\partial_x\Theta, \dot{\Theta}\}. \tag{B8}$$

The numerical budget is then evaluated as:

$$\frac{\Delta\Theta}{\Delta t} = -\left(u\frac{\partial\Theta}{\partial x}\right)_{\text{avg}} + \dot{\Theta}_{\text{avg}}. \tag{B9}$$

In this notation, the subscript "avg" explicitly denotes a time-averaged quantity; unless otherwise specified, all variables without this subscript are understood to be instantaneous snapshots. As shown in Fig. B1c, the budget achieves perfect closure at machine precision, validating the consistency of the framework before proceeding to anomaly decompositions.

d. Two Anomalous Temperature Budget Formulations

As introduced in Section 2, we evaluate the performance of the proposed framework using two distinct anomaly definitions. Specifically, we consider temperature anomalies defined relative to the climatological annual cycle, as well as those further detrended to isolate transient variability from long-term warming.

In this analytical configuration, the climatological mean of any physical quantity or flux term ϕ (representing either a snapshot field such as Θ or a time-averaged field such as Θ_{avg}) is calculated

by averaging the signal across N years for each specific seasonal phase $\tau \in [0, 1)$:

$$\overline{\phi}(x, z, \tau) = \frac{1}{N} \sum_{n=0}^{N-1} \phi(x, z, \tau + nT), \tag{B10}$$

where $T = 1$ is the annual period and $N = 40$. The corresponding anomaly is subsequently defined as $\phi' = \phi - \overline{\phi}$. This operator is applied consistently to all budget components to decompose the total variability into its seasonal cycle and anomalous perturbations.

1) The Anomaly Budget

In the first formulation, we consider the anomaly Θ' defined relative to the climatological annual cycle. To ensure numerical consistency within the discrete sampling framework, the tendency term is computed from instantaneous snapshots, while the forcing terms are derived from time-averaged diagnostics:

$$\frac{\Delta\Theta'}{\Delta t} = \frac{\Delta(\langle \frac{\partial\Theta}{\partial t} \rangle t)'}{\Delta t} - \left(u \frac{\partial \Theta'}{\partial x} \right)_{\text{avg}} - \left(u' \frac{\partial \overline{\Theta}}{\partial x} \right)_{\text{avg}} + \left(\overline{u' \frac{\partial \Theta'}{\partial x}} \right)_{\text{avg}} + \dot{\Theta}'_{\text{avg}}, \tag{B11}$$

where the right-hand side components represent the impact of the long-term mean tendency, and the theoretical decomposition of the anomalous advective and diabatic forcing, respectively.

However, in practical oceanographic applications—particularly when analyzing standard GCM outputs—high-frequency correlation terms (i.e., the time-average of instantaneous products of anomalies) are typically unavailable, because the instantaneous anomalies are unknowable at run time. To address this data constraint, we approximate the budget using resolved time-averaged fields:

$$\frac{\Delta\Theta'}{\Delta t} = \frac{\Delta(\langle \frac{\partial\Theta}{\partial t} \rangle t)'}{\Delta t} - u_{\text{avg}} \left(\frac{\partial \Theta}{\partial x} \right)'_{\text{avg}} - u'_{\text{avg}} \overline{\left(\frac{\partial \Theta}{\partial x} \right)_{\text{avg}}} + \overline{u'_{\text{avg}} \left(\frac{\partial \Theta}{\partial x} \right)'_{\text{avg}}} + \dot{\Theta}'_{\text{avg}} + \text{Res.} \tag{B12}$$

Specifically, the climatological eddy flux term is estimated from the resolved time-averaged variables through Reynolds decomposition:

$$\overline{u'_{\text{avg}} \left(\frac{\partial \Theta}{\partial x} \right)'_{\text{avg}}} = \overline{u_{\text{avg}} \left(\frac{\partial \Theta}{\partial x} \right)_{\text{avg}}} - \overline{u_{\text{avg}}} \overline{\left(\frac{\partial \Theta}{\partial x} \right)_{\text{avg}}}. \tag{B13}$$

This formulation mimics the typical archival strategy of ocean models, which prioritize time-mean velocity and tracer fields. Consequently, evaluating the budget in this manner provides a robust assessment of the framework's applicability to realistic GCM datasets where instantaneous cross-product terms are inaccessible.

2) The Detrended Anomaly Budget

The second formulation of $\tilde{\Theta}'$ is implemented by removing the locally defined long-term mean tendency from the total temperature. Applying the generalized anomaly operator to the detrended equations leads to a different partitioning:

$$\frac{\Delta\tilde{\Theta}'}{\Delta t} = -u_{\text{avg}}\left(\frac{\partial(\langle\frac{\partial\Theta}{\partial t}\rangle t)}{\partial x}\right)'_{\text{avg}} - u_{\text{avg}}\left(\frac{\partial\tilde{\Theta}}{\partial x}\right)'_{\text{avg}} - u'_{\text{avg}}\overline{\left(\frac{\partial\Theta}{\partial x}\right)}_{\text{avg}} + \overline{u'_{\text{avg}}\left(\frac{\partial\Theta}{\partial x}\right)'_{\text{avg}}} + \dot{\Theta}'_{\text{avg}} + \text{Res.} \quad \text{(B14)}$$

The first term on the right-hand side represents the advection of the long-term mean tendency anomaly. This term is vital for maintaining budget closure in regimes characterized by spatially varying warming rates. By contrasting Eqs. (B12) and (B14), we can discern how the explicit treatment of the long-term mean tendency modulates the interpretation of advective heat transport across different anomaly definitions.

e. Comparison of Budget Results

Figures B2a and B2b display the temporal evolution of the tendency terms for the anomaly and the detrended anomaly, respectively. Two primary findings emerge from this comparison. First, the anomaly tendency exhibits prominent "stair-step" discontinuities at the transition between annual cycles. This non-physical jump is explicitly contributed by the anomaly of the reconstructed long-term mean tendency [see the first term on the RHS of Eq. (15)] as shown in Figures B2c. Because the climatological baseline is re-centered annually, this tendency-related term manifests as a discrete impulse at each year-end boundary while remaining zero throughout the year. In contrast, the detrended anomaly $\tilde{\Theta}'$ is inherently free of such discontinuities; however, it remains influenced by the spatial heterogeneity of the long-term mean tendency [the first term on the RHS of Eq. (16)]. Unlike the localized annual jumps, this tendency-advection term exerts a persistent dynamical forcing on the detrended tendency that is active at every time step as shown in Figures B2d.

The second key result concerns the budget closure under the constraint of time-averaged outputs. As shown in Figs. B2o and B2p, both anomaly formulations achieve a near-zero residual (Res ≈ 0), validating the theoretical integrity of the proposed framework. This closure is particularly noteworthy because the right-hand side terms were calculated using time-averaged fields to derive the cross-product (eddy) terms, a process that typically neglects high-frequency correlations.

While these results confirm the mathematical consistency of our framework, we note that the high precision achieved here stems partly from the absence of high-frequency fluctuations in the analytical model. In realistic GCM diagnostics, even daily-averaged outputs may lead to non-negligible residuals due to the omission of sub-daily nonlinear interactions (e.g., diurnal cycles or high-frequency waves).[1] Nevertheless, the successful closure in this analytical testbed provides a robust benchmark, demonstrating that the framework itself does not introduce systemic errors when tendency anomalies and spatial heterogeneities are properly accounted for.

f. Discretization of Anomalous Water Mass Budgets

Here we detail the numerical implementation of the anomalous water mass framework within this analytical testbed. Following the theoretical derivation in Section 2, the anomalous water mass volume, $\mathcal{M}_{\geq}$, is defined by the domain where the temperature anomaly exceeds a specified threshold (i.e., $\Theta' \geq \Theta'_{\text{threshold}}$ or $\tilde{\Theta}' \geq \tilde{\Theta}'_{\text{threshold}}$). To maintain dynamical consistency, the volume tendency on the left-hand side (LHS) of the budget equation is calculated using snapshot temperature fields. Specifically, snapshot anomaly fields are projected onto the temperature coordinates to determine the instantaneous volume change.

On the RHS, the budgetary components are derived from time-averaged outputs. In this analytical setup, since explicit mass sources such as precipitation or evaporation are absent, the transformation is governed primarily by the transformation terms ($\mathcal{G}_M$) and the lateral volume flux terms ($\Psi_{\geq}$). These terms are computed by first using the time-averaged temperature anomaly field to identify the spatial domains (masks) where the anomaly exceeds the given threshold. Subsequently, the corresponding time-averaged physical fluxes within these identified domains are integrated. For the transformation terms involving derivatives with respect to the anomaly threshold (e.g., the

[1] For GCM simulations that are bit-wise reproducible, one could address this by running the model once to generate the climatological mean cycle and then re-run the model again a second time, using the now known climatological means for online diagnosis of instantaneous anomalies and the time-average of their products.

diabatic transformation $\mathcal{G}_{\dot{\Theta}'}$), we employ a second-order centered difference scheme:

$$\mathcal{G}_{\dot{\Theta}'}(\Theta'_n) = -\frac{\mathcal{F}(\Theta'_{n+1}) - \mathcal{F}(\Theta'_{n-1})}{\Theta'_{n+1} - \Theta'_{n-1}}, \quad \text{where} \quad \mathcal{F}(\Theta'_n) = \sum_{\mathbf{x}\in\Omega_{\geq}(\Theta'>\Theta'_n)} \dot{\Theta}'(\mathbf{x})\Delta V, \tag{B15}$$

where $\Omega_{\geq}(\Theta' > \Theta'_n)$ denotes the spatial domain where the temperature anomaly exceeds the threshold Θ'_n, and ΔV is the grid cell volume. This formulation represents the temperature anomaly flux across the Θ'_n isosurface, effectively capturing the diabatic forcing acting upon the anomalous water mass isosurface.

APPENDIX C

Anomalous Water Mass Budget in ECCO

ECCOv4r4 employs a rescaled height coordinate system ($z^* \equiv \frac{z-\eta}{H+\eta}H$), which allows the cell thickness $h = \Delta z\, s^*$ to evolve according to the time-varying barotropic scale factor $s^* = 1 + \eta/H$, where η is the sea surface height anomaly and H is the resting ocean depth. The potential temperature budget in ECCOv4 is diagnosed from available output in the extensive (cell-integrated) form:

$$\iiint \left[\frac{\partial(s^*\Theta)}{\partial t} + \nabla_h \cdot (s^*\mathbf{U}_h^{res}\,\Theta) + \frac{\partial(w^{res}\,\Theta)}{\partial z^*}\right] dA\, dz = \iiint \nabla \cdot \left(\mathbf{F}^{\Theta}_{\text{diff}} + \mathbf{F}^{\Theta}_{\text{forc}}\right) dA\, dz, \tag{C1}$$

where the dimensionless scaling factor s^* is separated from the fixed depth-coordinate cell volume $\mathrm{d}V_{\text{fixed}} \equiv dA\, dz$, following the conventions of Forget et al. (2015). Note that the diffusive flux $\mathbf{F}^{\Theta}_{\text{diff}}$ in the ECCO diagnostic output already incorporates the s^* scaling and that the velocity advecting tracers in ECCO should be interpreted as a residual-mean velocity, $\mathbf{U} = \mathbf{U}^r + \mathbf{U}^*$, in which $\mathbf{U}^r$ denotes the velocity resolved by ECCO's coarse grid and $\mathbf{U}^*$ denotes the eddy-induced bolus velocity arising from the Gent and Mcwilliams (1990)-type parameterization.

Water mass transformation analysis requires a conservation equation in terms of the material derivative of the temperature Θ, expressed in the intensive form:

$$\begin{aligned}\iiint \frac{D\Theta}{Dt}\, dV &\equiv \iiint \left(\frac{\partial \Theta}{\partial t} + \mathbf{U}\cdot\nabla\Theta\right) s^*\, dz\, dA \\ &= \iiint \left(s^*\frac{\partial \Theta}{\partial t} + s^*\mathbf{U}_h\cdot\nabla_h\Theta + w\frac{\partial \Theta}{\partial z^*}\right) dV_{\text{fixed}}.\end{aligned} \tag{C2}$$

Converting the temperature budget from its extensive form to its intensive form requires accounting for mass conservation. The local continuity equation takes the form

$$\frac{\partial s^*}{\partial t} + \nabla_h\cdot(s^*\mathbf{U}_h^r) + \frac{\partial w^r}{\partial z^*} = F, \tag{C3}$$

In the ECCO diagnostics, the freshwater source term F is absorbed into the surface vertical mass flux w, so that the local continuity equation reduces to:

$$\frac{\partial s^*}{\partial t} + \nabla\cdot(s^*\mathbf{U}^r) = 0. \tag{C4}$$

Since the eddy-induced bolus transport is non-divergent by construction, the continuity equation can also be expressed in terms of the residual velocity:

$$\frac{\partial s^*}{\partial t} + \nabla\cdot(s^*\mathbf{U}) = 0. \tag{C5}$$

To isolate the material derivative of Θ (scaled by s^*) from the ECCO budget, the integrand in Eq. (C1) is decomposed using the product rule as

$$s^*\frac{\partial \Theta}{\partial t} + s^*\mathbf{U}_h\cdot\nabla_h\Theta + w^r\frac{\partial \Theta}{\partial z^*} = -\Theta\left(\frac{\partial s^*}{\partial t} + \nabla_h\cdot(s^*\mathbf{U}_h) + \frac{\partial w}{\partial z^*}\right) + \nabla\cdot\left(\mathbf{F}_{\text{diff}}^{\Theta} + \mathbf{F}_{\text{forc}}\right). \tag{C6}$$

Substituting the continuity equation (C5) and dividing by s^* yields the compact form

$$\frac{\partial \Theta}{\partial t} + \mathbf{U}\cdot\nabla\Theta = \dot{\Theta}, \tag{C7}$$

where we introduce the material warming rate

$$\dot{\Theta} \equiv \frac{1}{s^*} \nabla \cdot (\mathbf{F}^{\Theta}_{\text{diff}} + \mathbf{F}^{\Theta}_{\text{forc}}). \tag{C8}$$

To identify the processes that transform anomalous water masses in ECCO, we need to re-express these budgets in terms of the material derivative of the temperature anomaly Θ'. Following the decomposition procedure described in section 2, the temperature anomaly Θ' is obtained by subtracting the climatological annual cycle. Taking the climatological mean of Eq. (C7):

$$\overline{\frac{\partial \Theta}{\partial t}} = -\overline{\mathbf{U}} \cdot \nabla \overline{\Theta} - \overline{\mathbf{U}' \cdot \nabla \Theta'} + \overline{\dot{\Theta}}. \tag{C9}$$

Subtracting Eq. (C9) from Eq. (C7) yields the anomaly tendency equation:

$$\frac{\partial \Theta'}{\partial t} = \frac{\partial \left(\langle \partial_t \Theta \rangle \, t \right)'}{\partial t} - \mathbf{U} \cdot \nabla \Theta' - \mathbf{U}' \cdot \nabla \overline{\Theta} + \overline{\mathbf{U}' \cdot \nabla \Theta'} + \left(\dot{\Theta} \right)'. \tag{C10}$$

Multiplying through by s^*, the s^*-weighted material derivative of Θ' becomes

$$s^* \frac{\partial \Theta'}{\partial t} + s^* \mathbf{U} \cdot \nabla \Theta' = s^* \left[\frac{\partial (\langle \partial_t \Theta \rangle \, t)'}{\partial t} - \mathbf{U}' \cdot \nabla \overline{\Theta} + \overline{\mathbf{U}' \cdot \nabla \Theta'} + \left(\dot{\Theta} \right)' \right]. \tag{C11}$$

The advective terms on the RHS of Eq. (C11) are written in advective form. However, since ECCO diagnostic output provides advective fluxes—and since $\nabla \cdot \mathbf{U} \neq 0$ in the z^* coordinate (unlike the Boussinesq case in section 2)—these terms must be converted to flux form by combining with the continuity equation (C5). We proceed term by term below.

(i) First advective term. The mean-gradient advection by the anomalous velocity is rewritten as

$$s^* \mathbf{U}' \cdot \nabla \overline{\Theta} = \nabla \cdot (s^* \mathbf{U}' \, \overline{\Theta}) - \overline{\Theta} \, \nabla \cdot (s^* \mathbf{U}'). \tag{C12}$$

(ii) Second advective term. Substituting Eq. (C9), the subseasonal covariance term becomes

$$
\begin{aligned}
s^*\overline{\mathbf{U}'\cdot\nabla\Theta'} &= s^*\left(-\overline{\frac{\partial\Theta}{\partial t}}-\overline{\mathbf{U}}\cdot\nabla\overline{\Theta}+\overline{\dot{\Theta}}\right)\\
&= -s^*\overline{\frac{\partial\Theta}{\partial t}}+s^*\overline{\dot{\Theta}}-\overline{s^*}\,\overline{\mathbf{U}}\cdot\nabla\overline{\Theta}-s^{*\prime}\overline{\mathbf{U}}\cdot\nabla\overline{\Theta}. \qquad \text{(C13)}
\end{aligned}
$$

To convert the last two terms into flux form in the Eq. (C13), we invoke the mean and anomalous continuity equations (C14) and (C15):

$$
\frac{\partial\overline{s^*}}{\partial t}+\nabla\cdot(\overline{s^*}\,\overline{\mathbf{U}})+\nabla\cdot\overline{(s^{*\prime}\mathbf{U}')}=0, \qquad \text{(C14)}
$$

$$
\frac{\partial s^{*\prime}}{\partial t}+\nabla\cdot(s^*\mathbf{U}')+\nabla\cdot(s^{*\prime}\overline{\mathbf{U}})-\nabla\cdot\overline{(s^{*\prime}\mathbf{U}')}=0, \qquad \text{(C15)}
$$

yielding

$$
\begin{aligned}
\overline{s^*}\,\overline{\mathbf{U}}\cdot\nabla\overline{\Theta} &= \nabla\cdot(\overline{s^*}\,\overline{\mathbf{U}}\,\overline{\Theta})-\overline{\Theta}\nabla\cdot(\overline{s^*}\,\overline{\mathbf{U}})\\
&= \nabla\cdot(\overline{s^*}\,\overline{\mathbf{U}}\,\overline{\Theta})+\overline{\Theta}\left(\frac{\partial\overline{s^*}}{\partial t}+\nabla\cdot\overline{(s^{*\prime}\mathbf{U}')}\right), \qquad \text{(C16)}
\end{aligned}
$$

$$
\begin{aligned}
s^{*\prime}\overline{\mathbf{U}}\cdot\nabla\overline{\Theta} &= \nabla\cdot(s^{*\prime}\overline{\mathbf{U}}\,\overline{\Theta})-\overline{\Theta}\nabla\cdot(s^{*\prime}\overline{\mathbf{U}})\\
&= \nabla\cdot(s^{*\prime}\overline{\mathbf{U}}\,\overline{\Theta})+\overline{\Theta}\left(\frac{\partial s^{*\prime}}{\partial t}+\nabla\cdot(s^*\mathbf{U}')-\nabla\cdot\overline{(s^{*\prime}\mathbf{U}')}\right). \qquad \text{(C17)}
\end{aligned}
$$

An additional relation is obtained from the climatological mean of Eq. (C1):

$$
\begin{aligned}
\overline{\frac{\partial(s^*\Theta)}{\partial t}} &= -\nabla\cdot\overline{(s^*\mathbf{U}\,\Theta)}+\overline{s^*\dot{\Theta}}\\
&= \overline{s^*\frac{\partial\Theta}{\partial t}}+\overline{\Theta\frac{\partial s^*}{\partial t}}\\
&= \overline{s^*}\,\overline{\frac{\partial\Theta}{\partial t}}+\overline{s^{*\prime}\left(\frac{\partial\Theta}{\partial t}\right)^{\prime}}+\overline{\Theta}\,\frac{\partial\overline{s^*}}{\partial t}+\overline{\Theta^{\prime}\frac{\partial s^{*\prime}}{\partial t}}. \qquad \text{(C18)}
\end{aligned}
$$

Combining Eqs. (C13)–(C18), the subseasonal covariance term is expressed as

$$s^*\overline{\mathbf{U}'\cdot\nabla\Theta'} = \nabla\cdot\overline{(s^*\mathbf{U}\Theta)} - \overline{s^*\dot{\Theta}} + \overline{s^{*\prime}\left(\frac{\partial\Theta}{\partial t}\right)'} + \overline{\Theta'\frac{\partial s^{*\prime}}{\partial t}} - s^{*\prime}\overline{\frac{\partial\Theta}{\partial t}} - \overline{\Theta}\frac{\partial s^{*\prime}}{\partial t}$$
$$+ s^*\overline{\dot{\Theta}} - \nabla\cdot(s^*\overline{\mathbf{U}}\,\overline{\Theta}) - \overline{\Theta}\nabla\cdot(s^*\mathbf{U}'). \tag{C19}$$

(iii) Sum of the two advective terms. Adding the negated first advective term [Eq. (C12)] and the second advective term [Eq. (C19)]:

$$\begin{aligned}
&- s^*\mathbf{U}'\cdot\nabla\overline{\Theta} + s^*\overline{\mathbf{U}'\cdot\nabla\Theta'} \\
&\quad = -\nabla\cdot(s^*\mathbf{U}'\overline{\Theta}) + \nabla\cdot\overline{(s^*\mathbf{U}\Theta)} - \nabla\cdot(s^*\overline{\mathbf{U}}\,\overline{\Theta}) \\
&\qquad + s^*\overline{\dot{\Theta}} - \overline{s^*\dot{\Theta}} + \overline{s^{*\prime}\left(\frac{\partial\Theta}{\partial t}\right)'} + \overline{\Theta'\frac{\partial s^{*\prime}}{\partial t}} - s^{*\prime}\overline{\frac{\partial\Theta}{\partial t}} - \overline{\Theta}\frac{\partial s^{*\prime}}{\partial t}.
\end{aligned} \tag{C20}$$

The anomalous diabatic term is

$$s^*\left(\dot{\Theta}\right)' = s^*\left(\dot{\Theta} - \overline{\dot{\Theta}}\right). \tag{C21}$$

Summing the last three RHS terms of Eq. (C11)—i.e., Eqs. (C20) and (C21)—yields

$$\begin{aligned}
&- s^*\mathbf{U}'\cdot\nabla\overline{\Theta} + s^*\overline{\mathbf{U}'\cdot\nabla\Theta'} + s^*\left(\dot{\Theta}\right)' \\
&\quad = -\nabla\cdot(s^*\mathbf{U}'\overline{\Theta}) + \nabla\cdot\overline{(s^*\mathbf{U}\Theta)} - \nabla\cdot(s^*\overline{\mathbf{U}}\,\overline{\Theta}) + (s^*\dot{\Theta})' \\
&\qquad + \overline{s^{*\prime}\left(\frac{\partial\Theta}{\partial t}\right)'} + \overline{\Theta'\frac{\partial s^{*\prime}}{\partial t}} - s^{*\prime}\overline{\frac{\partial\Theta}{\partial t}} - \overline{\Theta}\frac{\partial s^{*\prime}}{\partial t}.
\end{aligned} \tag{C22}$$

The last four terms in Eq. (C22), denoted F_{add}, can be simplified as follows:

$$\begin{aligned}
F_{\text{add}} &\equiv \overline{s^{*\prime}\left(\frac{\partial\Theta}{\partial t}\right)'} + \overline{\Theta'\frac{\partial s^{*\prime}}{\partial t}} - s^{*\prime}\overline{\frac{\partial\Theta}{\partial t}} - \overline{\Theta}\frac{\partial s^{*\prime}}{\partial t} \\
&= \overline{s^{*\prime}\frac{\partial\Theta'}{\partial t}} - \overline{s^{*\prime}\frac{\partial(\langle\partial_t\Theta\rangle\, t)'}{\partial t}} + \overline{\Theta'\frac{\partial s^{*\prime}}{\partial t}} - s^{*\prime}\frac{\partial\overline{\Theta}}{\partial t} - s^{*\prime}\frac{\partial(\langle\partial_t\Theta\rangle\, t)'}{\partial t} - \overline{\Theta}\frac{\partial s^{*\prime}}{\partial t} \\
&= \overline{\frac{\partial(s^{*\prime}\Theta')}{\partial t}} - \frac{\partial(s^{*\prime}\overline{\Theta})}{\partial t} - s^{*\prime}\frac{\partial(\langle\partial_t\Theta\rangle\, t)'}{\partial t}.
\end{aligned} \tag{C23}$$

Substituting into Eq. (C11), the anomaly budget becomes

$$s^*\frac{\partial\Theta'}{\partial t}+s^*\mathbf{U}\cdot\nabla\Theta'=\overline{s^*}\,\frac{\partial(\langle\partial_t\Theta\rangle\,t)'}{\partial t}-\nabla\cdot(s^*\mathbf{U}'\overline{\Theta})+\nabla\cdot\overline{(s^*\mathbf{U}\Theta)}-\nabla\cdot(s^*\overline{\mathbf{U}}\,\overline{\Theta})+(s^*\dot{\Theta})'+F_{s^*},\tag{C24}$$

where $F_{s^*}\equiv\overline{\frac{\partial(s^{*\prime}\Theta')}{\partial t}}-\frac{\partial(s^{*\prime}\overline{\Theta})}{\partial t}$ collects the residual terms arising from temporal correlations between $s^{*\prime}$ and Θ'.

Because the ECCO velocity output `UVELMASS` and `VVELMASS` already accounts for partial cells and time-varying grid-cell thickness, this diagnostic directly represents $s^*\mathbf{U}_h$. We therefore exploit the identity

$$\begin{aligned}-\nabla\cdot[(s^*\mathbf{U})'\overline{\Theta}]+\overline{\nabla\cdot[(s^*\mathbf{U})'\Theta']}&=-\nabla\cdot(s^*\mathbf{U}'\overline{\Theta})-\nabla\cdot[(s^{*\prime}\overline{\mathbf{U}})\,\overline{\Theta}]+\nabla\cdot[\overline{(s^{*\prime}\mathbf{U}')}\,\overline{\Theta}]\\&\quad+\nabla\cdot\overline{(s^*\mathbf{U}\Theta)}-\nabla\cdot(\overline{s^*}\,\overline{\mathbf{U}}\,\overline{\Theta})-\nabla\cdot[\overline{(s^{*\prime}\mathbf{U}')}\,\overline{\Theta}]\\&=-\nabla\cdot(s^*\mathbf{U}'\overline{\Theta})+\nabla\cdot\overline{(s^*\mathbf{U}\Theta)}-\nabla\cdot(s^*\overline{\mathbf{U}}\,\overline{\Theta}),\end{aligned}\tag{C25}$$

where the anomalous volume flux $(s^*\mathbf{U})'$ is computed directly from the ECCO output as $\texttt{UVELMASS}-\overline{\texttt{UVELMASS}}$. Substituting Eq. (C25) into Eq. (C24), the anomaly budget can be rewritten entirely in terms of ECCO diagnostics.

Accordingly, the ECCOv4r4-specific full-anomaly Θ'-water mass transformation, $\mathcal{G}_{\mathrm{M}}$, incorporates additional terms F_{s^*} relative to the standard formulation in Eq. (17):

$$\mathcal{G}_M=-\rho_0\,\partial_{\Theta'}\int_{\Omega_{\geq}\cap R}\left(\overline{s^*}\,\frac{\partial\left(\langle\partial_t\Theta\rangle\,t\right)'}{\partial t}-\nabla\cdot[(s^*\mathbf{U})'\overline{\Theta}]+\overline{\nabla\cdot[(s^*\mathbf{U})'\Theta']}+\nabla\cdot\left(\mathbf{F}^{\Theta}_{\mathrm{diff}}\right)'+\nabla\cdot\left(\mathbf{F}^{\Theta}_{\mathrm{forc}}\right)'+F_{s^*}\right)dV_{\mathrm{fixed}}.\tag{C26}$$

For clarity, we decompose the integrand into individual physical contributions and define the corresponding components of the Θ'-water mass transformation $\mathcal{G}_M$ as:

$$\begin{aligned}\mathcal{G}_M(\Theta')&=\mathcal{G}_{\dot{\Theta}'}+\mathcal{G}_{\langle\partial_t\Theta\rangle}+\mathcal{G}_{U'\overline{\Theta}}+\mathcal{G}_{\overline{U'\Theta'}}+\mathcal{G}_{\mathbf{F}_{s^*}}\\&=\mathcal{G}_{mix}+\mathcal{G}_Q+\mathcal{G}_{\langle\partial_t\Theta\rangle}+\mathcal{G}_{U'\overline{\Theta}}+\mathcal{G}_{\overline{U'\Theta'}}+\mathcal{G}_{\mathbf{F}_{s^*}}\end{aligned}\tag{C27}$$

Each term is defined as follows:

$$
\begin{aligned}
\mathcal{G}_{\langle\partial_t\Theta\rangle} &= -\rho_0\,\partial_{\Theta'}\int_{\Omega_{\geq}\cap R}\left[\overline{s^*}\,\frac{\partial\left(\langle\partial_t\Theta\rangle\,t\right)'}{\partial t}\right]dV_{\text{fixed}},\\
\mathcal{G}_{U'\overline{\Theta}} &= -\rho_0\,\partial_{\Theta'}\int_{\Omega_{\geq}\cap R}\left[-\nabla\cdot\left[(s^*\mathbf{U})'\overline{\Theta}\right]\right]dV_{\text{fixed}},\\
\mathcal{G}_{\overline{U'\Theta'}} &= -\rho_0\,\partial_{\Theta'}\int_{\Omega_{\geq}\cap R}\left[\overline{\nabla\cdot\left[(s^*\mathbf{U})'\Theta'\right]}\right]dV_{\text{fixed}},\\
\mathcal{G}_{mix} &= -\rho_0\,\partial_{\Theta'}\int_{\Omega_{\geq}\cap R}\nabla\cdot\left(\mathbf{F}^{\Theta}_{\text{diff}}\right)'dV_{\text{fixed}},\\
\mathcal{G}_{Q} &= -\rho_0\,\partial_{\Theta'}\int_{\Omega_{\geq}\cap R}\nabla\cdot\left(\mathbf{F}^{\Theta}_{\text{forc}}\right)'dV_{\text{fixed}},\\
\mathcal{G}_{\mathbf{F}_{s^*}} &= -\rho_0\,\partial_{\Theta'}\int_{\Omega_{\geq}\cap R}F_{s^*}\,dV_{\text{fixed}}.
\end{aligned}
\tag{C28}
$$

Collecting all contributions, the Θ'-water mass budget in ECCOv4r4 can be written as:

$$
\begin{aligned}
\frac{\partial}{\partial t}\mathcal{M}_{\geq}(\Theta') &= \mathcal{S}_{\geq}(\Theta') + \Psi_{\geq}(\Theta') + \mathcal{G}_{M}(\Theta')\\
&= \mathcal{S}_{\geq} + \Psi_{\geq} + \mathcal{G}_{mix} + \mathcal{G}_{Q} + \mathcal{G}_{\langle\partial_t\Theta\rangle} + \mathcal{G}_{U'\overline{\Theta}} + \mathcal{G}_{\overline{U'\Theta'}} + \mathcal{G}_{\mathbf{F}_{s^*}}.
\end{aligned}
\tag{C29}
$$

Equation (C29) generalizes the water mass budget to the full-anomaly framework and provides a dynamically consistent decomposition of surface forcing, lateral boundary transport, long-term mean trends, transient flux covariances, and diabatic processes.

The physical interpretation of each term is as follows. The first term on the RHS of Eq. (C29), $\mathcal{S}_{\geq}$, represents the change in water mass volume due to surface mass flux; in ECCOv4r4 this contribution arises solely from freshwater exchange across the air–sea interface. The second term, $\Psi_{\geq}$, denotes the advective transport of water mass across the fixed lateral boundaries of the control volume; for a global water mass analysis in which isothermal surfaces form closed interfaces, this boundary term vanishes identically. The third through fifth terms correspond to transformation processes analogous to those in the generalized Θ'-anomaly framework of Eq. (18): $\mathcal{G}_{\langle\partial_t\Theta\rangle}$ captures the contribution associated with the long-term linear temperature tendency; $\mathcal{G}_{U'\overline{\Theta}}$ arises from anomalous velocity advecting the climatological temperature field; and $\mathcal{G}_{\overline{U'\Theta'}}$ represents the water mass transformation driven by the climatological-mean transient advective heat flux, arising from the covariance between subseasonal velocity and temperature anomalies. The terms $\mathcal{G}_{mix}$ and $\mathcal{G}_{Q}$

account for interior diffusive mixing and surface heat flux anomalies, respectively, both of which contribute to diabatic water mass transformation $\mathcal{G}_{\dot{\Theta}'}$. Finally, $\mathcal{G}_{\mathbf{F}_{s^*}}$ represents the transformation induced by F_{s^*}, which arises from grid-cell volume fluctuations in the ECCOv4r4 framework.

In the numerical implication of Eq. (C29), The tendency of $\mathcal{M}_{\geq}$ is calculated by projecting on the daily snapshot temperature anomaly Θ'_{snap}. Because heat tendencies are not binned into temperature anomaly coordinates online, however, we project all of the daily-averaged RHS terms on the daily average Θ'_{avg} at the middle time of the two days.

Following an analogous decomposition, the ECCOv4r4-specific detrended anomaly $\tilde{\Theta}'$ budget is as follows:

$$s^* \frac{\partial \tilde{\Theta}'}{\partial t} + s^* \mathbf{U} \cdot \nabla \tilde{\Theta}' = -\nabla \cdot \left[s^* \mathbf{U} \left(\langle \partial_t \Theta \rangle t \right)' \right] - \nabla \cdot \left[(s^* \mathbf{U})' \overline{\Theta} \right] + \overline{\nabla \cdot \left[(s^* \mathbf{U})' \Theta' \right]} + \nabla \cdot (\mathbf{F}^{\Theta}_{\text{diff}})' + \nabla \cdot (\mathbf{F}^{\Theta}_{\text{forc}})' + F_{s^*} + \mathbf{F}_{\langle \partial_t \Theta \rangle}. \tag{C30}$$

where $\mathbf{F}_{\langle \partial_t \Theta \rangle} = \overline{s^*} \partial_t (\langle \partial_t \Theta \rangle t)' - \partial_t [s^* (\langle \partial_t \Theta \rangle t)']$, which can be equal to the first term in the RHS of the Eq. (C24) only when the s^* is time independent. Correspondingly, the ECCOv4r4-specific detrended anomaly $\tilde{\Theta}'-$water mass transformation, $\mathcal{G}_{\text{M}}$, is obtained by:

$$\mathcal{G}_M = -\rho_0 \partial_{\tilde{\Theta}'} \int_{\Omega_{\geq} \cap R} \Big(- \nabla \cdot \left[s^* \mathbf{U} \left(\langle \partial_t \Theta \rangle t \right)' \right] - \nabla \cdot \left[(s^* \mathbf{U})' \overline{\Theta} \right] + \overline{\nabla \cdot \left[(s^* \mathbf{U})' \Theta' \right]} + \nabla \cdot (\mathbf{F}^{\Theta}_{\text{diff}})' + \nabla \cdot (\mathbf{F}^{\Theta}_{\text{forc}})' + F_{s^*} + \mathbf{F}_{\langle \partial_t \Theta \rangle} \Big) dV_{\text{fixed}}. \tag{C31}$$

Analogous to the Θ' formulation in Eq. (C27), the total transformation rate is decomposed into distinct physical contributions:

$$\mathcal{G}_M(\tilde{\Theta}') = \mathcal{G}_{mix} + \mathcal{G}_Q + \mathcal{G}_{U(\langle \partial_t \Theta \rangle t)'} + \mathcal{G}_{U' \overline{\Theta}} + \mathcal{G}_{\overline{U' \Theta'}} + \mathcal{G}_{\mathbf{F}_{s^*}} + \mathcal{G}_{\mathbf{F}_{\langle \partial_t \Theta \rangle}}. \tag{C32}$$

All terms in Eq. (C32) share identical definitions with their counterparts in the Θ' budget [Eq. (C27)], with the exception of $\mathcal{G}_{U(\langle \partial_t \Theta \rangle t)'}$ and $\mathcal{G}_{\mathbf{F}_{\langle \partial_t \Theta \rangle}}$, which are specific to the detrended

anomaly framework. These two terms are defined as:

$$\mathcal{G}_{U(\langle\partial_t\Theta\rangle t)'} = -\rho_0\,\partial_{\tilde{\Theta}'}\int_{\Omega_{\geq}\cap R}\left(-\nabla\cdot\left[s^*\mathbf{U}\left(\langle\partial_t\Theta\rangle\, t\right)'\right]\right)dV_{\text{fixed}},$$
$$\mathcal{G}_{\mathbf{F}_{\langle\partial_t\Theta\rangle}} = -\rho_0\,\partial_{\tilde{\Theta}'}\int_{\Omega_{\geq}\cap R}\mathbf{F}_{\langle\partial_t\Theta\rangle}\,dV_{\text{fixed}}. \tag{C33}$$

Here, $\mathcal{G}_{U(\langle\partial_t\Theta\rangle t)'}$, analogous to its counterpart in Eq. (21), represents the water mass transformation arising from the spatial inhomogeneity of the linearly detrended temperature tendency. The term $\mathcal{G}_{\mathbf{F}_{\langle\partial_t\Theta\rangle}}$ serves as a correction term attributable to the temporal variability of s^*, and vanishes identically in the rigid-lid limit where grid-cell volumes are time-independent.

Collecting all contributions, the $\tilde{\Theta}'$ water mass budget in ECCOv4r4 is written as:

$$\frac{\partial}{\partial t}\mathcal{M}_{\geq}(\tilde{\Theta}') = \mathcal{S}_{\geq} + \Psi_{\geq} + \mathcal{G}_{mix} + \mathcal{G}_Q + \mathcal{G}_{U(\langle\partial_t\Theta\rangle t)'} + \mathcal{G}_{U'\overline{\Theta}} + \mathcal{G}_{\overline{U'\Theta'}} + \mathcal{G}_{\mathbf{F}_{s^*}} + \mathcal{G}_{\mathbf{F}_{\langle\partial_t\Theta\rangle}}. \tag{C34}$$

Compared with the standard anomalous water mass budget derived in Section2 under a fixed-volume framework, the ECCOv4r4 formulation is complicated by the temporal variability of the rescaled height coordinate s^*. Since s^* encodes the local volume expansion and contraction associated with sea surface height fluctuations in the z^* coordinate system, its variability modifies both the effective tracer tendency and the advective flux divergence within each grid cell. As a result, the ECCOv4r4 anomalous water mass transformation incorporates supplementary contributions — namely $\mathcal{G}_{\mathbf{F}_{s^*}}$ in the full-anomaly budget [Eq. (C29)], and additionally $\mathcal{G}_{\mathbf{F}_{\langle\partial_t\Theta\rangle}}$ in the detrended anomaly budget [Eq. (C34)] — arising from volume-modulation effects that are absent in the standard Boussinesq formulation with a rigid lid. In essence, while the dynamical structure of the anomaly budget remains consistent with the conventional framework, the temporal variability of s^* gives rise to a formally extended water mass transformation budget that is specific to the ECCOv4r4 z^*-coordinate system.

References

Bailey, S., H. F. Drake, L. K. Gruenburg, and R. P. Abernathey, 2024: The thermodynamics of the 2023 gulf-of-mexico marine heatwave. *Authorea Preprints*.

Bailey, S. T., C. S. Jones, R. P. Abernathey, A. L. Gordon, and X. Yuan, 2023: Water mass transformation variability in the Weddell Sea in ocean reanalyses. *Ocean Science*, **19 (2)**, 381–402, https://doi.org/10.5194/os-19-381-2023.

Bindoff, N. L., and Coauthors, 2007: Observations: oceanic climate change and sea level. *Climate change 2007: the physical science basis. Contribution of Working Group I*, 385–428.

Capotondi, A., and Coauthors, 2015: Understanding enso diversity. *Bulletin of the American Meteorological Society*, **96 (6)**, 921–938.

Drake, H. F., and Coauthors, 2025: Water mass transformation budgets in finite-volume generalized vertical coordinate ocean models. *Journal of Advances in Modeling Earth Systems*, **17 (3)**, e2024MS004 383.

Forget, G., J.-M. Campin, P. Heimbach, C. N. Hill, R. M. Ponte, and C. Wunsch, 2015: ECCO version 4: an integrated framework for non-linear inverse modeling and global ocean state estimation. *Geoscientific Model Development*, **8 (10)**, 3071–3104, https://doi.org/10.5194/gmd-8-3071-2015.

Forget, G., G. Maze, M. Buckley, and J. Marshall, 2011: Estimated seasonal cycle of north atlantic eighteen degree water volume. *Journal of Physical Oceanography*, **41 (2)**, 269–286.

Fukumori, I., O. Wang, and I. Fenty, 2021: Causal mechanisms of sea level and freshwater content change in the beaufort sea. *Journal of Physical Oceanography*, **51 (10)**, 3217–3234.

Gent, P. R., and J. C. Mcwilliams, 1990: Isopycnal mixing in ocean circulation models. *Journal of Physical Oceanography*, **20 (1)**, 150–155.

Griffies, S. M., R. C. Pacanowski, and R. W. Hallberg, 2000: Spurious Diapycnal Mixing Associated with Advection in a z -Coordinate Ocean Model. *Monthly Weather Review*, **128 (3)**, 538–564, https://doi.org/10.1175/1520-0493(2000)128⟨0538:SDMAWA⟩2.0.CO;2.

Groeskamp, S., S. M. Griffies, D. Iudicone, R. Marsh, A. G. Nurser, and J. D. Zika, 2019: The water mass transformation framework for ocean physics and biogeochemistry. *Annual review of marine science*, **11 (1)**, 271–305.

Hobday, A. J., and Coauthors, 2016: A hierarchical approach to defining marine heatwaves. *Progress in oceanography*, **141**, 227–238.

Iselin, C. O., 1939: The influence of vertical and lateral turbulence on the characteristics of the waters at mid-depths. *Eos, Transactions American Geophysical Union*, **20 (3)**, 414–417.

Lee, M.-M., A. C. Coward, and A. J. G. Nurser, 2002: Spurious Diapycnal Mixing of the Deep Waters in an Eddy-Permitting Global Ocean Model. *Journal of Physical Oceanography*, **32 (5)**, 1522–1535, https://doi.org/10.1175/1520-0485(2002)032⟨1522:SDMOTD⟩2.0.CO;2.

McPhaden, M. J., 1999: Genesis and evolution of the 1997-98 el niño. *Science*, **283 (5404)**, 950–954.

Megann, A., 2018: Estimating the numerical diapycnal mixing in an eddy-permitting ocean model. *Ocean Modelling*, **121**, 19–33, https://doi.org/10.1016/j.ocemod.2017.11.001.

Montgomery, R. B., 1958: Water characteristics of atlantic ocean and of world ocean. *Deep Sea Research (1953)*, **5 (2-4)**, 134–148.

Nurser, A., R. Marsh, and R. G. Williams, 1999: Diagnosing water mass formation from air–sea fluxes and surface mixing. *Journal of physical oceanography*, **29 (7)**, 1468–1487.

Santoso, A., M. J. Mcphaden, and W. Cai, 2017: The defining characteristics of enso extremes and the strong 2015/2016 el niño. *Reviews of Geophysics*, **55 (4)**, 1079–1129.

Speer, K., and G. Forget, 2013: Global distribution and formation of mode waters. *International geophysics*, Vol. 103, Elsevier, 211–226.

Speer, K. G., 1993: The deep silica tongue in the north atlantic. *Deep Sea Research Part I: Oceanographic Research Papers*, **40 (5)**, 925–936.

Sverdrup, H. U., M. W. Johnson, R. H. Fleming, and Coauthors, 1942: *The Oceans: Their physics, chemistry, and general biology*, Vol. 1087. Prentice-Hall New York.

Talley, L. D., and M. S. McCartney, 1982: Distribution and circulation of labrador sea water. *Journal of Physical Oceanography*, **12 (11)**, 1189–1205.

Trenberth, K. E., 1997: The definition of el nino. *Bulletin of the American Meteorological Society*, **78 (12)**, 2771–2778.

816 Walin, G., 1977: A theoretical framework for the description of estuaries. *Tellus*, **29 (2)**, 128–136,
817 https://doi.org/10.1111/j.2153-3490.1977.tb00716.x.

818 Walin, G., 1982: On the relation between sea-surface heat flow and thermal circulation in the
819 ocean. *Tellus*, **34 (2)**, 187–195.

820 Worthington, L., 1959: Oceanographic observations. *Geophys. Res. Pap*, **63**, 31–35.

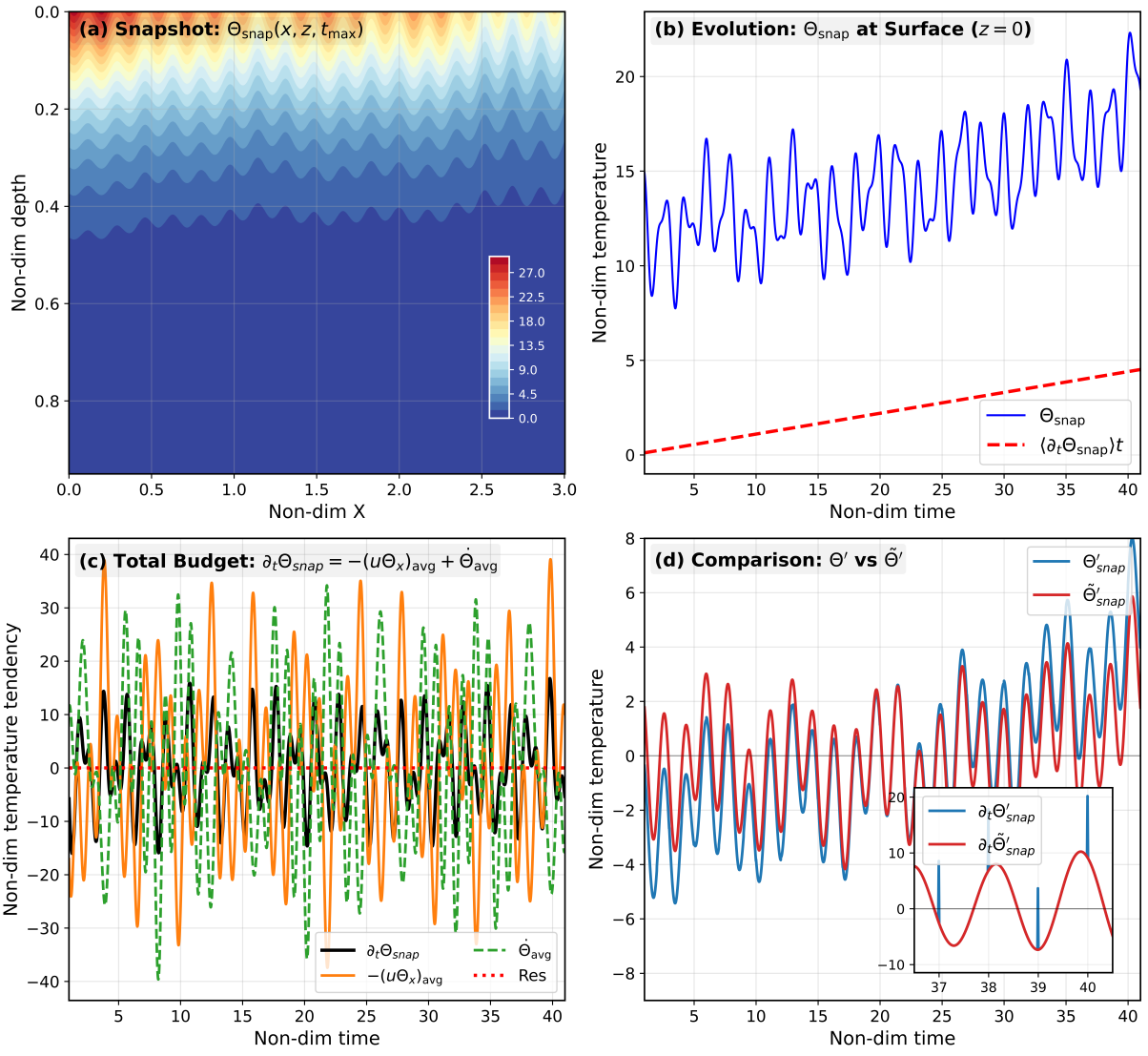

FIG. B1. (a) Snapshot of the simulated temperature field Θ. (b) Time series of temperature (blue solid) at a representative horizontal location, with the reconstructed linear long-term mean tendency component ($\langle \partial_t \Theta \rangle t$) overlaid in red dashed lines. (c) Validation of the instantaneous heat budget: the local temperature tendency ($\partial_t \Theta_{snap}$) (black solid) is balanced by the sum of the time-averaged advection (orange solid) and diabatic forcing (green dashed). The resulting residual (red dotted), representing the difference between the tendency and the total forcing, remains at machine precision. (d) Evolution of the temperature anomaly Θ' (blue) and the detrended anomaly $\tilde{\Theta}'$ (red). The inset magnification displays the corresponding temporal tendencies for both definitions; notably, the tendency exhibits characteristic "stair-step" discontinuities at the end of each year, arising from the re-centering of the long-term trend within the generalized climatological framework.

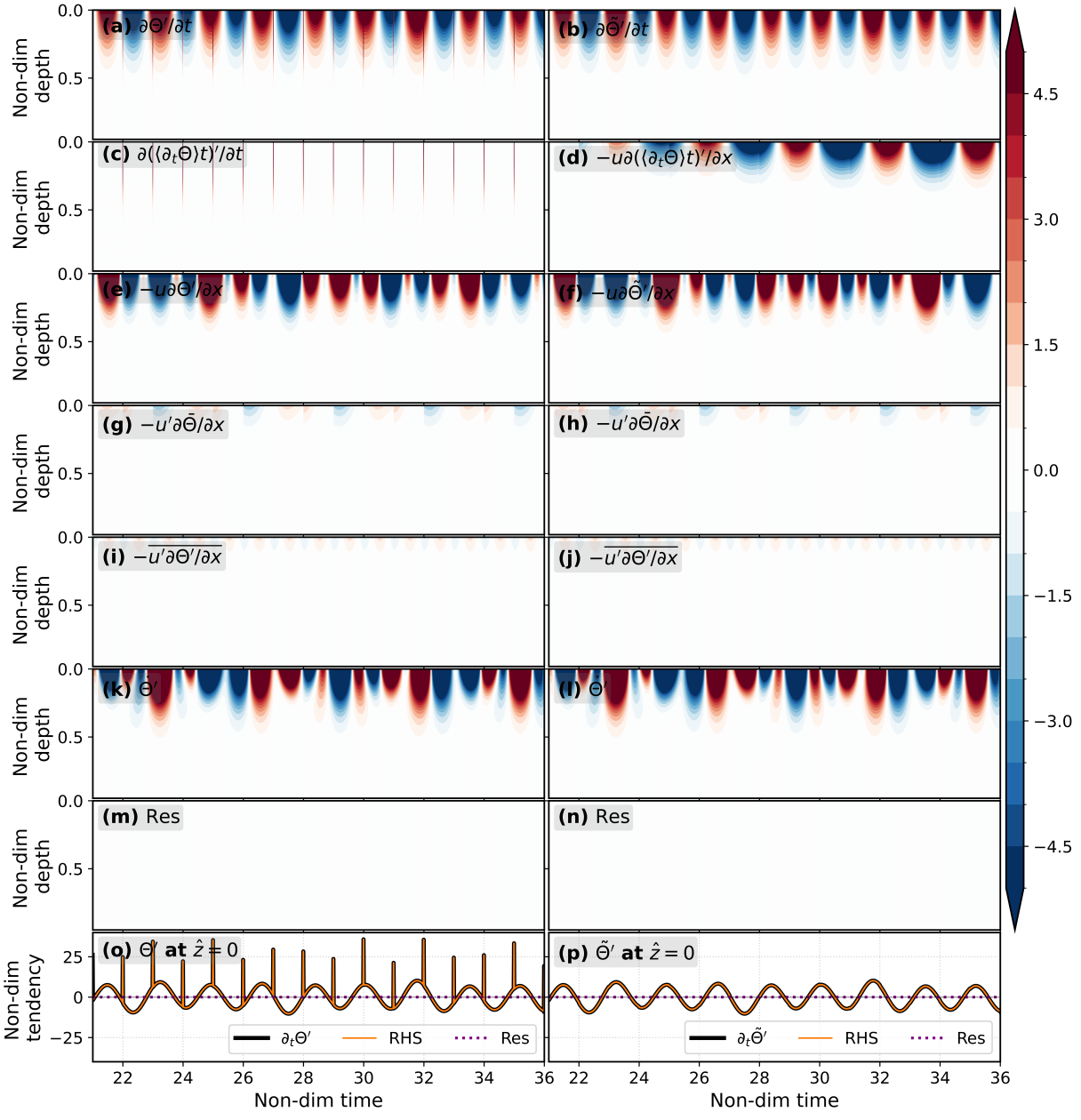

620 FIG. B2. The left column displays the time evolution of individual components within the anomaly budget
621 [Eq. (B12)], while the right column shows the corresponding evolution for the detrended wave anomaly budget
622 [Eq. (B14)].